Springer

Acta Mechanica Sinica

CrossMark click for updates

• INVITED REVIEW •

Acta Mech. Sin., Vol. 38, 222025 (2022)
https://doi.org/10.1007/s10409-022-22025-x

Micromechanics of composites with interface effects

Huiling Duan[1,2*], Jianxiang Wang[1,2], and Zhuping Huang[1]

[1] *State Key Laboratory for Turbulence and Complex Systems, Department of Mechanics and Engineering Science, Beijing Innovation Center for Engineering Science and Advanced Technology, College of Engineering, Peking University, Beijing 100871, China;*
[2] *Center for Applied Physics and Technology, Key Laboratory of High Energy Density Physics Simulations and IFSA Collaborative Innovation Center of the Ministry of Education, Peking University, Beijing 100871, China*

Received January 29, 2022; accepted March 25, 2022; published online online April 24, 2022

Interfaces that exist in composites greatly influence their mechanical and conductive properties. There are usually three interface models to characterize the elastic and conductive properties of the interface in composites. For elastic problems, they are the interface stress model (ISM), linear spring model (LSM), and interphase model. For conductive problems, they are the high conducting (HC) interface model, low conducting (LC) interface model, and interphase model. For elastic problems with the interface effects, they can be divided into two types. The first kind of elastic problem concerns the solution of boundary value problems and aims to predict the effective properties of composites with interface effects. The second kind of elastic problem concerns the surface/interface stress effects on the elastic properties of nanostructured materials, which is usually characterized by the ISM. In this paper, three aspects in the elastic problems with interface effects are first reviewed, i.e., equivalent relations among the three interface models, Eshelby formalism, and micromechanical frameworks. Special emphasis is placed on the ISM to show how classical models can be extended to the nano-scale by supplementing the interface elasticity to the basic equations of the classical elastic problems. Then, the conductive problems of the composites with the interface effects are also reviewed, and the general frameworks for predicting the effective conductivity of the composites are given. Finally, scaling laws depicting the size-dependent elastic and conductive properties of the composites are discussed.

Interface effect, Micromechanics, Composites, Effective properties, Scaling law

Citation: H. Duan, J. Wang, and Z. Huang, Micromechanics of composites with interface effects, Acta Mech. Sin. **38**, 222025 (2022), https://doi.org/10.1007/s10409-022-22025-x

1. Introduction

In real composites (or heterogeneous materials), factors such as processing can cause imperfect interfacial bonding between the matrix and the second phase inhomogeneities, which greatly affect the properties of electrical, thermal conduction, or elasticity [1]. For example, there is a temperature difference across the interface between the matrix and inhomogeneities when a heat flux is maintained, and this is called the Kapitza thermal boundary resistance in the field of thermal conduction [2]. Two kinds of models are often used to model the properties of interface in heterogeneous materials [3, 4], i.e., the interface models and the interphase model. In the interface models, there are discontinuities of quantities such as displacement, stress, and temperature across the interface, as shown in Fig. 1a. Among the interface models, two linear interface models, namely, the interface stress model (ISM) and linear spring model (LSM) for elasticity, or high conducting (HC) interface model and low conducting (LC) interface model for conductivity, have been extensively studied by researchers. For example, the LC interface (Kapitza resistance) in thermal conductivity has been studied by theory and experiment [5-7], and the ISM has been used to characterize the surface/interface stress effect on the mechanical properties of composites [8-10]. In the interphase model, the interface region is described as a layer between two dissimilar materials and has a finite thickness and given

*Corresponding author. E-mail address: hlduan@pku.edu.cn (Huiling Duan)
Executive Editor: Leiting Dong

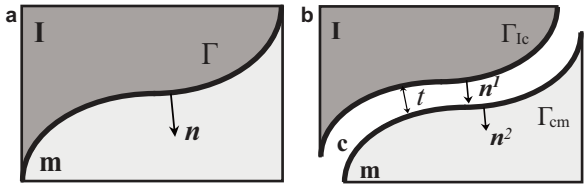

Figure 1 **a** Mathematical interface model and **b** interphase model.

material properties which are different from those of the surrounding materials, as shown in Fig. 1b. The interphase is usually viewed as nucleation, chemical reaction, or diffusion zone with homogeneous or variable material properties. At the matrix/interphase and interphase/inhomogeneity interfaces, perfect bonding is generally assumed.

For solid materials, material properties such as elastic modulus, and thermal conductivity, qualitatively or quantitatively affect the response of the material when it is subjected to given stimuli and constraints. For example, the elastic modulus influences the deformation under applied forces, and the thermal conductivity affects the amount of heat when fixed temperature gradients are applied. Material properties can be divided into many categories, of which equilibrium, steady state, and structure-sensitive material properties are the most commonly considered [11].

For the steady-state problem, the properties of heterogeneous materials can be characterized by effective ones. It is noted that the thermal conduction, diffusion, electrostatics, and magnetostatics are mathematically analogous, which are called the generalized conductivity problem. A list of quantities in these analogous problems is given in Hashin's work [12]. In addition, methods and models for solving elastic problems have corresponding methods and models for conductive problems. Thus, there is a strong relation between the issues of effective elastic properties and effective conductive properties, which has been summarized in Hashin's work [12].

The effective properties of heterogeneous materials have been discussed in a number of reviews [11-13]. This review paper is concerned with the theoretical aspects of heterogeneous materials with equilibrium, steady-state, structure-sensitive, and effective properties. In addition, this paper addresses itself to the issues in the presence of interface effects, and is concerned essentially with the relationships between the behavior of heterogeneous materials and their structures with interface effects (Fig. 2). Next, a brief outline of this review paper is given. Section 2 deals with the interface models and their equivalent relations for the elasticity problem. Section 3 gives the Eshelby formalism and micromechanical frameworks with three interface effects. Section 4 illustrates a new micromechanical scheme and predicts the effective elastic modulus of multiphase composites. Section 5 reviews the works related to the effective conductivity of heterogeneous materials with interface effects. Section 6 provides two kinds of scaling law governing the size-dependent effective properties of the heterogeneous materials with interface effects.

2. Interface models for elastic problems

There is a large amount of literature on interface effects that exist in solid mechanics, which can be divided into two categories. Works in the first category are concerned with the solution of boundary value problems and aim to estimate the effective elastic modulus of the heterogeneous materials with interface effects. Imperfect interface bonding may exist in heterogeneous materials [14], which greatly affects their properties [15-20]. For instance, the grain boundary sliding at room temperature has been reported in polycrystalline and granular media [16, 21]. The interfaces in the nanocrystalline materials can modulate the deformation of the materials through the grain-boundary sliding and separation [22-24]. It has also been pointed out that grain boundary softening is important for both nanocrystalline materials and conventional materials [25].

Based on the interface models and interphase model mentioned in Sect. 1, the elastic fields and effective elastic properties of the conventional composites have been extensively studied in the consideration of the interface bonding conditions [8, 9, 15, 26-47]. Based on the atomic simulation of Schiøtz et al. [24], Jiang and Weng [48] simulated the grain-boundary region of nanocrystalline materials as interphase and used a three-phase model to predict the effective mechanical properties of nanocrystalline materials. Wei and Anand [22] described the thin grain-boundary region by an elastic-plastic interface model and predicted the effective properties through a crystal-plasticity model. Tan et al. [49] predicted the effective modulus of particle-reinforced composites with a piecewise linear cohesive interface model [49, 50].

Works in the second category are concerned with the ISM characterizing the elastic properties of nano-structured materials [51-57]. Gibbs (1906) first introduced the surface/interface stress in solids, and the study of surface/interface stress has developed steadily since then [58-63]. Surface/interface stress can be expressed as the surface/interface excess of bulk stress [64, 65] or defined by the Shuttleworth equation [58]. The atomistic interpretation of the interface stress has been presented by Nix and Gao [66]. There are two kinds of interface stress discussed in the literature. One is called coherent interface and assumes that there is no atomic bond breakage in the interface and the abutting solids have equal tangential strain. The other assumes that

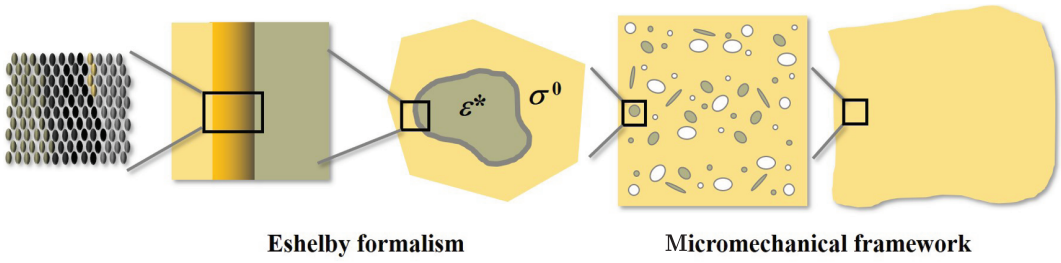

Figure 2 Illustration of studies on composite considering interface effects.

the atomic bonds in the interface may break as slipping across the interface, and there are different tangential strains in the two solids [67]. In general, coherent interfaces often exist in materials under various conditions [68].

Surface/interface stress can move atoms away from the equilibrium positions they normally occupy in the macroscopic assemblies [69, 70], and the elastic properties of nanostructures are influenced by the change in atomic distance. Attempts through continuum theory and molecular dynamic simulation have been made to show how surface stress can affect the elastic properties of nanobeams, nanowires, nanoplates, and nanocomposites [10, 34, 35, 71-78]. Miller and Shenoy [71] used a continuum model and atomistic simulation to depict the surface stress influence on the elastic properties of nanosized plates and beams. Zhou and Huang [79] combined molecular statics and *ab initio* calculations to study the elastic properties of nanoplates and found that the surface can soften or stiffen the nanoplates. Jing et al. [74] found that the apparent Young's modulus of nanowires decreases with the increased diameter of the nanowires via theory and experiments. The size dependence of the apparent Young's modulus is caused by the surface effect of nanowires, including the effects of the surface stress, the oxidation layer, and the surface roughness. Mancarella et al. [10, 35] experimentally tested Young's modulus of soft composites with microscale droplets, and have found that the effective elastic properties can be significantly enhanced by microscale droplets due to the interface stress.

Gurtin and Ian Murdoch [80] proposed the first continuum model to show the influence of surface stress effect on the elastic properties of nanostructures, and it has been further developed to calculate the elastic properties of nanostructured materials [32, 71, 81-83]. Miller and Shenoy [71] found that the results for nanobeams and nanowires calculated by the continuum model are similar to those obtained by the atomistic simulations. Steigmann and Ogden [84] further considered the effect of bending resistance of elastic films attached to solid boundary surfaces and generalized the Gurtin-Murdoch theory to the Steigmann-Ogden interface model, which has been widely applied in calculating the effective properties of nanocomposites [36, 37].

When calculating the effective properties of nanocomposites, the Eshelby formalism is essential [85, 86]. The Eshelby formalism [85-87] includes the strain field of inclusion under uniform eigenstrain in an infinite elastic medium, the elastic field of inhomogeneity in an infinite medium under arbitrary uniform far-field stress, and strain energy in solids containing inhomogeneities. Here, an inclusion is a subdomain subjected to an eigenstrain in a solid with the same elastic properties of the solid, and an inhomogeneity is a region in a solid whose elastic properties are different from the surrounding solid [85, 88]. An inhomogeneous inclusion denotes an inhomogeneity subjected to an eigenstrain. Many researchers have made attempts to obtain the Eshelby formalism for the nano-inhomogeneity. Sharma et al. [89, 90] analyzed the influence of interface stress on the elastic field of a spherical inhomogeneity embedded in an infinite medium. The inhomogeneity is subjected to a uniform dilatational eigenstrain, and the infinite medium is subjected to a hydrostatic remote loading. Duan et al. [32] gave the Eshelby formalism of the nano-inhomogeneity. To predict the effective properties of the heterogeneous materials containing nano-inhomogeneities, micromechanical frameworks are required. Many attempts have been made to give the micromechanical frameworks for estimating the effective properties such as the elastic modulus and thermal expansion coefficients [43, 83, 91-93]. For example, Duan et al. [83] provided a general micromechanical framework for estimating the effective elastic modulus of heterogeneous materials with the interface stress effect. Duan et al. [91] further gave the effective elastic modulus of nanochannel-array materials and found that rationally designing the pore surface elasticity and surface coating can make nanochannel-array materials stiffer than the parent materials. The intrinsic relations governing these effective properties have also been widely studied by researchers [45, 46, 94-96].

In other respects, the surface stress effect has been considered in a finite element method (FEM) by Gao et al. [97], and the developed FEM has been applied in analyzing the elastic properties of nano-structured materials. Fang and Liu [98]

investigated the size-dependent interaction between the edge dislocation and the circular nano-inhomogeneity. The influence of the surface/interface elasticity on the nanoparticles embedded in a semi-infinite elastic medium has been studied by Mi and Kouris [99].

Since the interface effects play an important role in determining the elastic properties of nano-structure materials, illustrations of how to consider the interface effects within the classical framework and interface models characterizing the elastic properties of the interface are summarized in the following.

2.1 Three kinds of interface models for elastic problems

To estimate the effective elastic properties of nano-structured materials, boundary-value problems of thermoelasticity are first required to be solved, which are given by

$$\begin{aligned} &\nabla\cdot\boldsymbol{\sigma}^k=\mathbf{0},\\ &\boldsymbol{\sigma}^k=\mathbf{C}^k:\boldsymbol{\varepsilon}^k-\Delta T\mathbf{d}^k,\\ &\boldsymbol{\varepsilon}^k=\frac{1}{2}\left(\nabla\otimes\mathbf{u}^k+\mathbf{u}^k\otimes\nabla\right). \end{aligned} \tag{1}$$

Here, superscripts $k=\mathrm{I}$ and $k=\mathrm{m}$ represent the quantities in Ω_{I} (inhomogeneity) and Ω_{m} (matrix), respectively. $\boldsymbol{\sigma}$, $\mathbf{u}$, and $\boldsymbol{\varepsilon}$ are the stress tensor, displacement tensor, and strain tensor, respectively. $\mathbf{C}$ and $\mathbf{d}$ are the stiffness tensor and the stress-temperature tensor. ΔT is the temperature difference. When considering the isotropic case, we have $\mathbf{d}^k=d^k\mathbf{I}^{(2)}$. Here, $d^k=\alpha_k(3\lambda_k+2\mu_k)$, and α_k, λ_k and μ_k are the thermal expansion coefficient and elastic moduli, respectively. $\mathbf{I}^{(2)}$ is the second-order identity tensor in three-dimensional space. It is noted that the inhomogeneity considered here can be the spherical inhomogeneity or the cylindrical fiber.

In addition to Eq. (1), the corresponding interface conditions need to be supplemented when considering the interface effects. In the following, three kinds of interface models are illustrated, i.e., the ISM, LSM, and the interphase model.

2.1.1 ISM

The ISM is described by the generalized Young-Laplace equation and continuous displacement condition, which are expressed as [80, 100]

$$[\mathbf{u}]=\mathbf{0},\quad \mathbf{n}\cdot[\boldsymbol{\sigma}]=-\nabla_S\cdot\boldsymbol{\tau}. \tag{2}$$

$[\cdot]=(\text{out})-(\text{in})$ represents the discontinuity of a quantity across the interface. $\mathbf{n}$ is the unit vector normal to the coherent interface Γ, and $\nabla_S\cdot\boldsymbol{\tau}$ is the interface divergence of $\boldsymbol{\tau}$ [80]. When the interface is isotropic, the interface stress $\boldsymbol{\tau}$ can be related to the interface strain $\boldsymbol{\varepsilon}^s$, and the relation is expressed as

$$\boldsymbol{\tau}=2\mu_s\boldsymbol{\varepsilon}^s+\lambda_s(\mathrm{tr}\boldsymbol{\varepsilon}^s)\mathbf{1}-\Delta T\mathbf{d}_0. \tag{3}$$

Here, λ_s and μ_s are the elastic moduli of the interface, and $\mathbf{d}_0$ is the stress-temperature tensor. $\mathbf{1}$ is the second-order identity tensor in the two-dimensional space. When the interface is isotropic, $\mathbf{d}_0=d_0\mathbf{1}$ and $d_0=\alpha_s\kappa_s$. α_s is the thermal expansion coefficient of the interface, and $\kappa_s=2(\mu_s+\lambda_s)$. When the interface is coherent, $\boldsymbol{\varepsilon}^s$ equals the tangential strain in the abutting bulk materials. Equation (2) can be applied to model the excess of the bulk stress at an interface [65], in which the interface modulus and thermal expansion coefficient may be obtained using atomistic simulations [69, 70, 82]. Equation (2) can also be applied to provide an accurate simulation of the thin and stiff interphase [101], in which the interface modulus and thermal expansion coefficient can be determined by the modulus, thickness, and thermal expansion coefficient of the interphase.

2.1.2 LSM

In the LSM, the interface conditions can be given by [96]

$$[\boldsymbol{\sigma}]\cdot\mathbf{n}=\mathbf{0},\quad [\mathbf{u}]=\boldsymbol{\beta}\cdot\boldsymbol{\sigma}\cdot\mathbf{n}+\boldsymbol{\gamma}\cdot\Delta T. \tag{4}$$

$\boldsymbol{\beta}=\beta_n\mathbf{n}\otimes\mathbf{n}+\beta_s\mathbf{s}\otimes\mathbf{s}+\beta_t\mathbf{t}\otimes\mathbf{t}$ is a second-order tensor with β_n, β_s, and β_t representing the interface elastic parameters. $\mathbf{n}$, $\mathbf{s}$, and $\mathbf{t}$ are the unit normal and tangential vectors of the interface, respectively. $\boldsymbol{\gamma}=\gamma_n\mathbf{n}+\gamma_s\mathbf{s}+\gamma_t\mathbf{t}$ is the displacement-temperature vector of the interface with γ_n, γ_s, and γ_t being the interface thermoelastic parameters. Duan and Karihaloo [96] proposed that the thermoelastic term expressed by $\boldsymbol{\gamma}\cdot\Delta T$ should be included in its constitutive description. When $\boldsymbol{\beta}\to 0$, $\boldsymbol{\gamma}\to 0$, the interface displacement jumps disappear and a perfect bonding is formed at the interface. When $\boldsymbol{\beta}\to\infty$, $\boldsymbol{\gamma}\to\infty$, the interface tractions disappear, which represents the debonding of the adjoining media. When parameters in $\boldsymbol{\beta},\boldsymbol{\gamma}$ are finite and positive, they define an imperfect interface. The linear-spring model described by Eq. (4) is generally applied to model thin and compliant interphase, in which the interface parameters can be obtained by the modulus, thickness, and thermal expansion coefficient of the interphase.

2.1.3 Interphase model

The interface models, i.e., the ISM and the LSM, are two-phase models with the volume fraction of the interface region in the heterogeneous material being zero, whereas the interphase model is a three-phase model and is composed of the inhomogeneity, interphase of given thickness, and matrix with perfect bonding assumed at both the inhomogene-

ity/interphase interface $\Gamma_{\rm Ic}$ and the interphase/matrix interface $\Gamma_{\rm cm}$, which are expressed as

$$\mathbf{n}^j \cdot [\boldsymbol{\sigma}^j] = \mathbf{0}, \quad [\mathbf{u}^j] = \mathbf{0}, \qquad j = 1, 2, \tag{5}$$

where the superscript $j = 1$ and 2 denote the interfaces $\Gamma_{\rm Ic}$ and $\Gamma_{\rm cm}$, and $\mathbf{n}$ is the unit normal vector of the interface as shown in Fig. 1b. The interphase can be either uniform or gradient [102, 103]. Hashin and Rosen [104] applied the interphase model into calculating the elastic moduli of fiber composites. Lutz and Zimmerman [105] studied the effect of the localized interphase on the overall mechanical properties of a particulate composite. The interphase model has been used to estimate the mechanical properties of nanocrystalline with the interphase parameters obtained by the inter-atomic potential simulation [106].

2.2 Equivalent relations among three interface models

Now that both the interface models (e.g., ISM and LSM) and interphase model can be applied to model the interface properties, then the question arises: is it possible to replace the three-phase model (i.e., interphase model) with a two-phase model (i.e., interface model) if given a thin interface between two media? This question has been answered affirmatively by many researchers [29, 107].

It is often convenient in obtaining the solutions to the boundary-value problems of composites by replacing the interphase with a proper interface model [108, 109]. There is extensive literature on this topic to date, from the pioneering works of Sanchez-Palencia [110], and Pham Huy and Sanchez-Palencia [111] in conduction, to those works in elasticity [112, 113], and to the recent works in discrete lattice model representation [114]. Fairly comprehensive references on simulating the interphase through interface models can be found in the works of Rubin et al. [109,115-117]. Benveniste and Miloh [115] derived different regimes of imperfect interfaces in a curved thin layer by utilizing the asymptotic expansion of displacement and stress. Rubin and Benveniste [109] formulated the Cosserat shell model for thin interfaces to uniformly simulate several regimes of imperfect interfaces. Although the Cosserat shell model can successfully model the imperfect interfaces, its construction requires the appropriate assumption of strain energies for the shell-like interface. Hashin [116] and Benveniste [117] adopted the Talyor expansion of the relevant quantities within the interphase to represent the interphase uniformly through the interface and obtained a complete spectrum of its material properties.

The idea to derive an interface model from the interphase based on Taylor expansions originated from Hashin et al. [29, 118, 119], and then was used by many researchers. For example, Miloh and Benveniste [120] used it to simulate the highly conducting thin interphases; Hashin [116, 121] used it for a thin interphase which has arbitrary conductivity and elastic moduli; and Wang et al. [101] used it to obtain the ISM from a thin and stiff interphase. It is noted that Bövik et al. [118, 119] successfully represented the isotropic thin interphase with a LSM for studying the scatting properties of inhomogeneities. Benveniste [117] generalized the study of Bövik [119] and achieved the representation of a thin anisotropic three-dimensional curved interphase through an interface in the conductive and elastic settings. To the authors' knowledge, the method of Taylor expansions is extensively used in describing the equivalent relations among the interphase model and interface models, and the representative works of this method are Hashin [116], and Benveniste [117]. However, it is emphasized that although Hashin [116] and Benveniste [117] used the same tool of Taylor expansions, they are different in derivations of their models. More detailed discussion can be found in Benveniste's work [117].

As mentioned above, the ISM and LSM are two extensively used interface models for simulating the interface bonding conditions in heterogeneous materials and characterizing the elastic properties of the nano-structured materials. It can be seen from Eqs. (3) and (4) that the quantities in these interface models, such as elastic modulus and elastic field, depend on the elastic modulus and thermal expansion coefficient of the interface and need to be determined experimentally. However, since the interface regions have a volume fraction of zero in these interface models, the experimental characterization of these interface quantities is difficult. Because the ISM and LSM are often used to model the behavior of thin interphases [29, 101, 122, 123], these quantities in the interface models can be derived from the equivalent relations between the interface models and the thin interphase. In the following, we only give some essential results of the equivalent relations between these two models and the interphase model by using the method of Taylor expansions of Hashin [116].

Consider thin interphase with a thickness t between the matrix and the inhomogeneity. The interfaces between the interphase and inhomogeneity, and between the interphase and the matrix are denoted by $\Gamma_{\rm Ic}$ and $\Gamma_{\rm cm}$, respectively. Spherical particles are used here as an example to illustrate the process, and the process for cylindrical fiber is similar. There exist displacement and stress differences (Δu_j and $\Delta\sigma_{rj}$, $j = r, \theta, \varphi$) across the interphase, which can be accurately approximated by the following relations [116]:

$$\begin{aligned} \Delta u_j &= u_j^{\rm c}(R+t) - u_j^{\rm c}(R) = t\, u_{j,r}^{\rm c}\big|_{\Gamma_{\rm Ic}}, \\ \Delta\sigma_{rj} &= \sigma_{rj}^{\rm c}(R+t) - \sigma_{rj}^{\rm c}(R) = t\, \sigma_{rj,r}^{\rm c}\big|_{\Gamma_{\rm Ic}}. \end{aligned} \tag{6}$$

The subscript $\Gamma_{\rm Ic}$ represents the quantities at the interface $\Gamma_{\rm Ic}$,

and the sub- and superscript "c" represents the quantities of the interphase. For the interface models, there are displacement and stress jumps ($[u_j]$ and $[\sigma_{rj}]$) across the interface (Γ), which are given by

$$[u_j] \equiv u_j^{\mathrm{m}}(\Gamma) - u_j^{\mathrm{p}}(\Gamma), \quad [\sigma_{rj}] \equiv \sigma_{rj}^{\mathrm{m}}(\Gamma) - \sigma_{rj}^{\mathrm{p}}(\Gamma). \tag{7}$$

Then, the equivalent relations between the interface models and interphase models can be obtained by equaling the displacement and stress differences (Δu_j and $\Delta\sigma_{rj}$) across the interphase to the displacement and stress jumps ($[u_j]$ and $[\sigma_{rj}]$) across the interface, i.e.,

$$[u_j] = \Delta u_j, \quad [\sigma_{rj}] = \Delta\sigma_{rj}. \tag{8}$$

The displacement and stress differences across a thin and stiff interphase can be characterized as $\Delta u_j = 0$, $\Delta\sigma_{rj} =$ finite, which is similar to the description of the ISM, i.e., Eq. (2). Letting $[u_j] = u_j^{\mathrm{m}}(\Gamma) - u_j^{\mathrm{p}}(\Gamma) = 0$, $[\sigma_{rj}] = \sigma_{rj}^{\mathrm{m}}(\Gamma) - \sigma_{rj}^{\mathrm{p}}(\Gamma) = \Delta\sigma_{rj}$, then we can obtain the equivalent relations between a thin and stiff interphase and an ISM. The elastic modulus and thermal expansion coefficient of the equivalent ISM are given by

$$\lambda_s = \frac{2\mu_{\mathrm{c}}\nu_{\mathrm{c}}t}{1-\nu_{\mathrm{c}}},\ \mu_s = \mu_{\mathrm{c}}t,\ \kappa_s = 2(\lambda_s+\mu_s),\ \alpha_s = \alpha_{\mathrm{c}}. \tag{9}$$

Here, ν_{c} is the Poisson ratio of the interphase.

The displacement and stress differences across a thin and compliant interphase can be characterized as $\Delta u_j =$ finite, $\Delta\sigma_{rj} = 0$, and are similar to the LSM described by Eq. (4). Letting $[u_j] = u_j^{\mathrm{m}} - u_j^{\mathrm{p}} = \Delta u_j$, $[\sigma_{rj}] = \sigma_{rj}^{\mathrm{m}}(\Gamma) - \sigma_{rj}^{\mathrm{p}}(\Gamma) = 0$, then the equivalent relations between a thin and compliant interphase and a LSM are assured. The elastic modulus and thermal expansion coefficient of the equivalent LSM are given by

$$\beta_n = \frac{t}{\lambda_{\mathrm{c}}+2\mu_{\mathrm{c}}},\ \beta_t = \frac{t}{\mu_{\mathrm{c}}},\ \gamma = \frac{\alpha_{\mathrm{c}}(1+\nu_{\mathrm{c}}) - 2\alpha_{\mathrm{p}}\nu_{\mathrm{c}}}{1-\nu_{\mathrm{c}}}t. \tag{10}$$

Equation (10) describes the case of spherical particles, and can describe the case of cylindrical fibers when $2\alpha_{\mathrm{p}}$ in the expression is replaced by α_{fT}.

Although the method of Taylor expansions has been successfully applied in estimating the relationship between the interface model and interphase model, it usually assumes that the interphase is thin and uniform without considering the complexity of the interphase structure [29,101,122,123]. For the naturally thin interphase layer, the first order of Taylor expansions is usually precise. However, higher orders of Taylor expansions are required to maintain accuracy when studying the thick interphase [124-127]. For thick and complex microstructured interphase, the interface position might not be the mid-layer, which will influence the behavior of the interface model [128]. Furthermore, the method of Taylor expansions usually corresponds to small-strain linear elasticity, which might be inapplicable for large deformations. More attention should be paid to these problems [128].

3. Eshelby formalism and micromechanical frameworks

3.1 Eshelby formalism

The Eshelby formalism [85-87] is the basis for solving many elastic problems in composite mechanics, solid state physics, and materials science. However, the classical Eshelby formalism does not include the influence of the interface, which limits its application in nano-structured materials. In the following, the Eshelby formalisms considering three interface effects are presented.

3.1.1 Eshelby formalism for ISM

Consider a spherical inhomogeneous inclusion with interface effect described by the ISM. The spherical inhomogeneous inclusion is a spherical inhomogeneity embedded in an infinite matrix and is subjected to a uniform eigenstrain. The total strain $\boldsymbol{\varepsilon}^k(\mathbf{x})$ in the spherical inhomogeneous inclusion ($k = \mathrm{I}$) and in the matrix ($k = \mathrm{m}$) can be related to the prescribed uniform eigenstrain $\boldsymbol{\varepsilon}^*$ in the inhomogeneity through the following expression [32]:

$$\boldsymbol{\varepsilon}^k(\mathbf{x}) = \mathbf{S}^k(\mathbf{x}) : \boldsymbol{\varepsilon}^*, \quad k = \mathrm{I}, \mathrm{m}, \quad \forall \mathbf{x} \in \Omega_{\mathrm{I}} + \Omega_{\mathrm{m}}, \tag{11}$$

where $\mathbf{S}^k(\mathbf{x})$ is the Eshelby tensor and $\mathbf{x}$ is the position vector. Similarly, the total stresses $\boldsymbol{\sigma}^k(\mathbf{x})$ in the two phases can be related to the prescribed uniform remote stress $\boldsymbol{\sigma}^0$ through the following expression:

$$\boldsymbol{\sigma}^k(\mathbf{x}) = \mathbf{T}^k(\mathbf{x}) : \boldsymbol{\sigma}^0, \quad k = \mathrm{I}, \mathrm{m}, \quad \forall \mathbf{x} \in \Omega_{\mathrm{I}} + \Omega_{\mathrm{m}}, \tag{12}$$

where $\mathbf{T}^k(\mathbf{x})$ is the stress concentration tensor. The Eshelby tensors $\mathbf{S}^k(\mathbf{x})$ and the stress concentration tensors $\mathbf{T}^k(\mathbf{x})$ are transversely isotropic with any radius being the symmetrical axis. Thus, Walpole notation [129] can be used to represent them. The Eshelby tensor is expressed as [32]

$$\mathbf{S}^k(\mathbf{r}) = \widetilde{\mathbf{S}}^k(r)\cdot\widetilde{\mathbf{E}}^{\mathrm{T}}, \quad k = \mathrm{I}, \mathrm{m}, \tag{13}$$

in which

$$\widetilde{\mathbf{S}}^k(r) = \begin{bmatrix} S_1^k(r) & S_2^k(r) & S_3^k(r) & S_4^k(r) & S_5^k(r) & S_6^k(r) \end{bmatrix}, \tag{14}$$

and

$$\widetilde{\mathbf{E}} = \begin{bmatrix} \mathbf{E}^1 & \mathbf{E}^2 & \mathbf{E}^3 & \mathbf{E}^4 & \mathbf{E}^5 & \mathbf{E}^6 \end{bmatrix}, \tag{15}$$

where $\mathbf{r} = r\mathbf{n}$ is the position vector. r is the distance from the material point where the Eshelby tensor is calculated to the center of the spherical inhomogeneity, and $\mathbf{n}$ is the unit vector along the radius of the spherical inhomogeneity. $\mathrm{S}_q^k(r)$ ($q = 1, 2, \cdots, 6$) are the components of the Eshelby tensor and are functions of r, and $\mathbf{E}^p$ ($p = 1, 2, \cdots, 6$) are the elementary tensors defined by Walpole [129]. Similarly, the stress concentration tensors can also be represented by the Walpole notation, which are expressed as [32]

$$\mathbf{T}^k(\mathbf{r}) = \widetilde{\mathbf{T}}^k(r)\cdot\widetilde{\mathbf{E}}^{\mathrm{T}}, \quad k = \mathrm{I}, \mathrm{m}, \tag{16}$$

in which

$$\widetilde{\mathbf{T}}^k(r) = \left[\begin{array}{cccccc} T_1^k(r) & T_2^k(r) & T_3^k(r) & T_4^k(r) & T_5^k(r) & T_6^k(r) \end{array}\right]. \tag{17}$$

The detailed procedure to obtain the results in Eqs. (13)- (17) can be found in the work of Duan et al. [32].

It is noted that the Eshelby tensor $\mathbf{S}^{\mathrm{I}}(\mathbf{x})$ and the stress concentration tensor $\mathbf{T}^{\mathrm{I}}(\mathbf{x})$ in the inhomogeneity with the interface stress are generally position-dependent, which are different from the classical results. The size dependence of the Eshelby tensor is represented by two non-dimensional parameters $\kappa_s^r = l_\kappa/R$ and $\mu_s^r = l_\mu/R$, with R being the radius of the spherical inhomogeneity, and $l_\kappa = \kappa_s/\mu_{\mathrm{m}}$ and $l_\mu = \mu_s/\mu_{\mathrm{m}}$ being two intrinsic length scales. The Eshelby tensor for the case without the interface stress effects can be directly obtained by setting $\kappa_s = 0$ and $\mu_s = 0$ or by letting $R \to \infty$, which is a constant tensor. When the spherical inhomogeneity is subjected to a dilatational eigenstrain given by $\boldsymbol{\varepsilon}^*{=}\varepsilon^0\mathbf{I}^{(2)}$, the total strain of the inhomogeneity is expressed as $\boldsymbol{\varepsilon}^{\mathrm{I}}{=}\varepsilon^0\mathbf{S}^{\mathrm{I}} : \mathbf{I}^{(2)}$. Since $\mathbf{S}^{\mathrm{I}} : \mathbf{I}^{(2)}$ is a constant tensor whether there is interface effect or not, the stress field in the inhomogeneity is homogeneous, which confirms the results of Sharma et al. [89].

The strain energy given by the Eshelby formalism is important for analyzing the mechanical properties of the heterogeneous materials [32, 87], since it converts the volume integration to surface integration. Consider a spherical inhomogeneity embedded in an elastic matrix occupying the volume of V. ∂V is the external surface of the matrix, and Γ is the interface between the inhomogeneity and the matrix. When a uniform strain boundary condition $\mathbf{u} = \boldsymbol{\varepsilon}^0 \cdot \mathbf{x}$ is applied at the external surface of the matrix, and the elastic strain energy U of the heterogeneous material given by the Eshelby formula with the interface stress effect can be expressed as

$$U = U_0 + \frac{1}{2}\int_\Gamma \Big(\mathbf{n}\cdot\boldsymbol{\sigma}\cdot\mathbf{u}^0 - \mathbf{u}\cdot\boldsymbol{\sigma}^0\cdot\mathbf{n}\Big)\mathrm{d}\Gamma, \tag{18}$$

in which

$$U_0 = \frac{1}{2}\int_V \boldsymbol{\sigma}^0 : \boldsymbol{\varepsilon}^0 \mathrm{d}V. \tag{19}$$

where $\boldsymbol{\varepsilon}^0$ is a constant strain tensor. $\boldsymbol{\sigma}$ and $\mathbf{u}$ are the stress tensor and displacement vector at Γ, and the stress tensor is evaluated on the matrix side. $\boldsymbol{\sigma}^0$ and $\mathbf{u}^0$ represent the stress tensor and displacement vector in a homogeneous body consisting only of the matrix materials, which occupies the region of the same volume as that of the heterogeneous material. When a uniform stress boundary condition $\Sigma = \boldsymbol{\sigma}^0 \cdot \mathbf{m}(\mathbf{x})$ is applied at the external surface of the matrix, the strain energy U of the heterogeneous material given by the Eshelby formula with the interface stress effect can be written as

$$U = U_0 + \frac{1}{2}\int_\Gamma \Big(\mathbf{n}\cdot\boldsymbol{\sigma}^0\cdot\mathbf{u} - \mathbf{u}^0\cdot\boldsymbol{\sigma}\cdot\mathbf{n}\Big)\mathrm{d}\Gamma, \tag{20}$$

where $\mathbf{m}(\mathbf{x})$ is the outward unit normal vector to the external surface of the matrix ∂V.

3.1.2 *Eshelby formalism for LSM and interphase model*

When considering a spherical inhomogeneous inclusion embedded in an infinite matrix with the interface effect described by the LSM, the corresponding Eshelby tensor and stress concentration tensor have the same forms as Eqs. (13) and (16). The size dependence of the Eshelby tensor is represented by two non-dimensional parameters l_r/R and l_θ/R with R being the radius of the spherical inhomogeneity, and $l_r = \beta_{\mathrm{n}}\mu_{\mathrm{m}}$ and $l_\theta = \beta_{\mathrm{s}}\mu_{\mathrm{m}}$ being two intrinsic lengths scales.

When the heterogeneous material is subjected to a uniform strain boundary condition $\mathbf{u} = \boldsymbol{\varepsilon}^0 \cdot \mathbf{x}$, the elastic strain energy given by the Eshelby formula with the LSM can be written as

$$U = U_0 + \frac{1}{2}\int_\Gamma \Big(\mathbf{n}\cdot\boldsymbol{\sigma}\cdot\mathbf{u}^0 - \mathbf{u}\cdot\boldsymbol{\sigma}^0\cdot\mathbf{n}\Big)\mathrm{d}\Gamma, \tag{21}$$

where the displacement tensor $\mathbf{u}$ is evaluated on the matrix side. The elastic strain energy given by the Eshelby formula for the LSM under $\Sigma = \boldsymbol{\sigma}^0 \cdot \mathbf{m}(\mathbf{x})$ is expressed as

$$U = U_0 + \frac{1}{2}\int_\Gamma \Big(\mathbf{n}\cdot\boldsymbol{\sigma}^0\cdot\mathbf{u} - \mathbf{u}^0\cdot\boldsymbol{\sigma}\cdot\mathbf{n}\Big)\mathrm{d}\Gamma. \tag{22}$$

Consider a spherical inhomogeneity embedded in an infinite matrix, which has uniform interphase or graded interphase whose elastic modulus is only the function of radius r. The Eshelby tensors and the stress concentration tensors in the inhomogeneity, the interphase, and the matrix can be expressed by Eqs. (13) and (16), since the problem considered here is both geometrically and physically symmetric and these tensors are all transversely isotropic tensors. Duan et al. [130] gave the results of the case that the moduli of the interphase are power-law functions of r, i.e., $\kappa_{\mathrm{c}}(r) = \kappa_0 r^Q$, $\mu_{\mathrm{c}}(r) = \mu_0 r^Q$, ν_{c} = constant, where κ_0, μ_0, and Q are constants. If $Q = 0$, the results degenerate into those of uniform interphase. By making the modulus

of the infinite matrix tend to infinity or vanish, the Eshelby tensors with uniform (or graded) interphase can be applied to the finite spherical inhomogeneity with fixed displacement or traction-free boundary conditions.

3.2 Micromechanical frameworks

As mentioned above, three interface models, namely, ISM, LSM, and interphase model, are extensively used to model the interface properties of the heterogeneous materials. Next, the interface effects on the effective elastic properties of the heterogeneous materials are discussed. Interface effects affect the effective modulus of heterogeneous materials in two ways. The average stress (strain) in the inhomogeneity is affected by the interface bonding conditions and can be considered by using the stress (strain) concentration tensor in the inhomogeneity. The discontinuities in the quantities across the interface result in additional stress (strain) when calculating the volume average of the stress (strain), which can be accounted for by using the stress (strain) concentration tensor at the interface. Then, the effective mechanical properties of heterogeneous materials can be modeled by the micromechanical schemes after accounting for interfacial effects in the calculations of volume-averaged quantities in these schemes. Benveniste [131] proposed a general framework for considering displacement discontinuities, which has been applied to calculate the effective modulus of heterogeneous materials with displacement discontinuity by Hashin [29]. Duan et al. [83] gave a general framework for considering stress discontinuity and using this framework to predict the effective mechanical properties of the heterogeneous materials with interface stress effects. In the following, a brief illustration of the micromechanical framework for predicting the effective mechanical properties of heterogeneous materials with three types of interface models is given.

A representative volume element (RVE) of the heterogeneous material is considered here, which is composed of the inhomogeneities Ω_{I} and the matrix Ω_{m}. V is the volume of the RVE, and ∂V is the external boundary of the RVE. $\mathbf{C}_k$ and $\mathbf{D}_k$ are the stiffness tensor and the compliance tensor in the inhomogeneity ($k = \mathrm{I}$) and matrix ($k = \mathrm{m}$). Assume that the heterogeneous material is statistically homogeneous, and the average strain $\bar{\boldsymbol{\varepsilon}}$ and average stress $\bar{\boldsymbol{\sigma}}$ are defined as [115]

$$\begin{aligned}\bar{\boldsymbol{\varepsilon}} &= \frac{1}{2V}\int_{\partial V}(\mathbf{m}\otimes\mathbf{u}+\mathbf{u}\otimes\mathbf{m})\,\mathrm{d}A,\\ \bar{\boldsymbol{\sigma}} &= \frac{1}{V}\int_{\partial V}(\boldsymbol{\sigma}\cdot\mathbf{m})\otimes\mathbf{x}\,\mathrm{d}A,\end{aligned} \tag{23}$$

where $\mathbf{m}(\mathbf{x})$ is the normal vector on the external surface of the RVE. Then, the effective elastic properties of the two-phase heterogeneous materials can be estimated by applying the homogeneous boundary conditions to the external surface ∂V, which are respectively defined as

$$\mathbf{u} = \boldsymbol{\varepsilon}^0\cdot\mathbf{x} \qquad \text{or} \qquad \Sigma = \boldsymbol{\sigma}^0\cdot\mathbf{m}(\mathbf{x}), \tag{24}$$

where $\boldsymbol{\varepsilon}^0$ and $\boldsymbol{\sigma}^0$ are constant strain and stress tensors. When considering the interface effects, discontinuities in the displacement vector or traction vector across the interface should be included, and then the average strain and stress of the heterogeneous materials are given by

$$\bar{\boldsymbol{\varepsilon}} = (1-f_{\mathrm{I}})\,\bar{\boldsymbol{\varepsilon}}^{\mathrm{m}} + f_{\mathrm{I}}\,\bar{\boldsymbol{\varepsilon}}^{\mathrm{I}} + \frac{f_{\mathrm{I}}}{2V_{\mathrm{I}}}\int_{\Gamma}(\mathbf{n}\otimes[\mathbf{u}]+[\mathbf{u}]\otimes\mathbf{n})\,\mathrm{d}\Gamma, \tag{25}$$

and

$$\bar{\boldsymbol{\sigma}} = (1-f_{\mathrm{I}})\,\bar{\boldsymbol{\sigma}}^{\mathrm{m}} + f_{\mathrm{I}}\,\bar{\boldsymbol{\sigma}}^{\mathrm{I}} + \frac{f_{\mathrm{I}}}{V_{\mathrm{I}}}\int_{\Gamma}([\boldsymbol{\sigma}]\cdot\mathbf{n})\otimes\mathbf{x}\,\mathrm{d}\Gamma, \tag{26}$$

where $[\boldsymbol{\sigma}] = \boldsymbol{\sigma}^{\mathrm{m}} - \boldsymbol{\sigma}^{\mathrm{I}}$, $[\mathbf{u}] = \mathbf{u}^{\mathrm{m}} - \mathbf{u}^{\mathrm{I}}$. In Eqs. (25) and (26), $[\boldsymbol{\sigma}] = \mathbf{0}$ is used for the case considering the linear-spring model, and $[\mathbf{u}] = \mathbf{0}$ is used for the case considering the ISM.

3.2.1 *Micromechanical frameworks with ISM*

When a displacement boundary condition $\mathbf{u} = \boldsymbol{\varepsilon}^0\cdot\mathbf{x}$ is applied to the RVE, one can predict the effective stiffness tensor of the heterogeneous materials with the ISM, which is given by

$$\bar{\mathbf{C}} = \mathbf{C}_{\mathrm{m}} + f_{\mathrm{I}}\,(\mathbf{C}_{\mathrm{I}} - \mathbf{C}_{\mathrm{m}}) : \mathbf{R} + f_{\mathrm{I}}\mathbf{C}_{\mathrm{m}} :: \mathbf{G}. \tag{27}$$

The strain concentration tensors $\mathbf{R}$ and $\mathbf{G}$ are defined as

$$\bar{\boldsymbol{\varepsilon}}^{\mathrm{I}} = \mathbf{R} : \boldsymbol{\varepsilon}^0, \quad \frac{1}{V_{\mathrm{I}}}\int_{\Gamma}([\boldsymbol{\sigma}]\cdot\mathbf{n})\otimes\mathbf{x}\,\mathrm{d}\Gamma = \mathbf{C}_{\mathrm{m}} : \mathbf{G} : \boldsymbol{\varepsilon}^0. \tag{28}$$

When a traction boundary $\Sigma = \boldsymbol{\sigma}^0\cdot\mathbf{m}(\mathbf{x})$ is applied, the effective compliance tensor is

$$\bar{\mathbf{D}} = \mathbf{D}_{\mathrm{m}} + f_{\mathrm{I}}\,(\mathbf{D}_{\mathrm{I}} - \mathbf{D}_{\mathrm{m}}) : \mathbf{U} - f_{\mathrm{I}}\,\mathbf{D}_{\mathrm{m}} : \mathbf{W}, \tag{29}$$

where the stress concentration tensors $\mathbf{U}$ and $\mathbf{W}$ are defined as

$$\bar{\boldsymbol{\sigma}}^{\mathrm{I}} = \mathbf{U} : \boldsymbol{\sigma}^0, \quad \frac{1}{V_{\mathrm{I}}}\int_{\Gamma}([\boldsymbol{\sigma}]\cdot\mathbf{n})\otimes\mathbf{x}\,\mathrm{d}\Gamma = \mathbf{W} : \boldsymbol{\sigma}^0. \tag{30}$$

3.2.2 *Micromechanical frameworks with LSM*

Likewise, under the displacement boundary condition $\mathbf{u} = \boldsymbol{\varepsilon}^0\cdot\mathbf{x}$, the effective stiffness tensor of the heterogeneous materials with the LSM is

$$\bar{\mathbf{C}} = \mathbf{C}_{\mathrm{m}} + f_{\mathrm{I}}\,(\mathbf{C}_{\mathrm{I}} - \mathbf{C}_{\mathrm{m}}) : \mathbf{M} - f_{\mathrm{I}}\,\mathbf{C}_{\mathrm{m}} : \mathbf{N}, \tag{31}$$

in which two strain concentration tensors $\mathbf{M}$ and $\mathbf{N}$ are expressed as

$$\bar{\boldsymbol{\varepsilon}}^{\mathrm{I}} = \mathbf{M} : \boldsymbol{\varepsilon}^0, \quad \frac{1}{2V_{\mathrm{I}}}\int_{\Gamma}(\mathbf{n}\otimes[\mathbf{u}]+[\mathbf{u}]\otimes\mathbf{n})\,\mathrm{d}\Gamma = \mathbf{N} : \boldsymbol{\varepsilon}^0. \tag{32}$$

Under the traction boundary condition $\Sigma = \boldsymbol{\sigma}^0 \cdot \mathbf{m}(\mathbf{x})$, the effective compliance tensor of the the heterogeneous materials with the LSM is

$$\bar{\mathbf{D}} = \mathbf{D}_\mathrm{m} + f_\mathrm{I}\,(\mathbf{D}_\mathrm{I} - \mathbf{D}_\mathrm{m}) : \mathbf{P} + f_\mathrm{I}\mathbf{D}_\mathrm{m} : \mathbf{Q}, \tag{33}$$

in which two stress concentration tensors $\mathbf{P}$ and $\mathbf{Q}$ are given by

$$\begin{aligned} &\bar{\boldsymbol{\sigma}}^\mathrm{I} = \mathbf{P} : \boldsymbol{\sigma}^0, \\ &\frac{1}{2V_\mathrm{I}}\int_\Gamma (\mathbf{n}\otimes[\mathbf{u}] + [\mathbf{u}]\otimes\mathbf{n})\,\mathrm{d}\Gamma = \mathbf{D}_\mathrm{m} : \mathbf{Q} : \boldsymbol{\sigma}^0. \end{aligned} \tag{34}$$

It is noted that Eqs. (27) and (29) for the ISM, and Eqs. (31) and (33) for the LSM can be used to estimate the effective elastic properties of heterogeneous materials by using the micromechanical frameworks, such as the dilute concentration approximation, generalized self-consistent method (GSCM) [132], and Mori-Tanaka method (MTM) [133], once the strain and stress concentration tensors in these expressions are obtained.

3.2.3 *Micromechanical frameworks with interphase model*

When considering an RVE of the heterogeneous materials containing inhomogeneities with interphases, let f_I, f_c, and f_m be the volume fraction of the inhomogeneities, interphases, and matrix. The stiffness and compliance tensors of the interphase are $\mathbf{C}^\mathrm{c}$ and $\mathbf{D}^\mathrm{c}$, respectively. Then, the volume average strain and stress of the RVE can be respectively expressed as

$$\begin{aligned} \bar{\boldsymbol{\varepsilon}} &= f_\mathrm{m}\bar{\boldsymbol{\varepsilon}}^\mathrm{m} + f_\mathrm{I}\bar{\boldsymbol{\varepsilon}}^\mathrm{I} + f_\mathrm{c}\bar{\boldsymbol{\varepsilon}}^\mathrm{c}, \\ \bar{\boldsymbol{\sigma}} &= f_\mathrm{m}\bar{\boldsymbol{\sigma}}^\mathrm{m} + f_\mathrm{I}\bar{\boldsymbol{\sigma}}^\mathrm{I} + f_\mathrm{c}\bar{\boldsymbol{\sigma}}^\mathrm{c} \\ &= f_\mathrm{m}\mathbf{C}_\mathrm{m} : \bar{\boldsymbol{\varepsilon}}^\mathrm{m} + f_\mathrm{I}\mathbf{C}_\mathrm{I} : \bar{\boldsymbol{\varepsilon}}^\mathrm{I} + f_\mathrm{c}\mathbf{C}_\mathrm{c} : \bar{\boldsymbol{\varepsilon}}^\mathrm{c}. \end{aligned} \tag{35}$$

Therefore, the effective stiffness tensor can be calculated by the following expressions:

$$\begin{aligned} \bar{\mathbf{C}} : \bar{\boldsymbol{\varepsilon}} = \mathbf{C}_\mathrm{m} : \bar{\boldsymbol{\varepsilon}}^\mathrm{m} &+ f_\mathrm{I}\,(\mathbf{C}_\mathrm{I} - \mathbf{C}_\mathrm{m}) : \bar{\boldsymbol{\varepsilon}}^\mathrm{I} \\ &+ f_\mathrm{c}\,(\mathbf{C}_\mathrm{c} - \mathbf{C}_\mathrm{m}) : \bar{\boldsymbol{\varepsilon}}^\mathrm{c}. \end{aligned} \tag{36}$$

Within the above micromechanical frameworks of the interface and interphase models, many researchers have estimated the effective mechanical properties of particle- and fibre-reinforced composites, including those of Qiu et al. [134,135]. Hashin and Monteiro [135] used the above framework and the GSCM to estimate the effective elastic properties of the concrete, which is a kind of three-phase composites consisting of the cement paste matrix, discrete rock inhomogeneities, and an interfacial transition zone (ITZ) between them. Zhang et al. [19] predicted the thermal damage of hybrid fiber-reinforced concrete based on the LSM model.

4. A unified scheme for multiphase composites with interface effects

So far, to predict the effective mechanical properties of linear composites, many micromechanical frameworks have been proposed [136-140], as well as the mechanical behaviors of nonlinear composites [141-143], such as the GSCM [132, 144], Torquato's third-order approximation (TOA) [145], and MTM [133, 146]. Although these micromechanical frameworks can provide good estimations close to the numerical results [144], some limitations need to be considered in their applications. For example, the MTM may underestimate the effective shear modulus of the heterogeneous materials when the hard inhomogeneities are in a high volume fraction [144, 147]. From an overall perspective, it is considered that the GSCM and TOA can provide the best estimations [4, 148]. Moreover, the GSCM takes the matrix atmosphere into account, which may greatly improve the accuracy of the estimated results [148]. In this section, we reviewed a unified GSCM scheme for multiphase composites with interface effects based on the Eshelby formalism for the three-phase configuration.

Consider a heterogeneous material consisting of the randomly distributed spherical inhomogeneities and a continuous matrix, whose effective stiffness tensor $\bar{\mathbf{C}}$ and compliance tensor $\bar{\mathbf{D}}$ can be given by [149]

$$\bar{\mathbf{C}} = \mathbf{C}_\mathrm{m} + f_\mathrm{I}(\mathbf{C}_\mathrm{I} - \mathbf{C}_\mathrm{m}) : \bar{\mathbf{E}}^\mathrm{I}, \tag{37}$$

and

$$\bar{\mathbf{D}} = \mathbf{D}_\mathrm{m} + f_\mathrm{I}(\mathbf{D}_\mathrm{I} - \mathbf{D}_\mathrm{m}) : \bar{\mathbf{T}}^\mathrm{I}, \tag{38}$$

where $\mathbf{C}$ and $\mathbf{D}$ are the stiffness tensor and the compliance tensor with subscripts "I" and "m" representing the inhomogeneities and the matrix. f_I is the volume fraction of the inhomogeneities. $\bar{\mathbf{E}}^\mathrm{I}$ in Eq. (37) and $\bar{\mathbf{T}}^\mathrm{I}$ in Eq. (38) are the strain concentration tensor and stress concentration tensor in the inhomogeneities, respectively, and are defined as

$$\bar{\boldsymbol{\varepsilon}}^\mathrm{I} = \bar{\mathbf{E}}^\mathrm{I} : \boldsymbol{\varepsilon}^0, \quad \bar{\boldsymbol{\sigma}}^\mathrm{I} = \bar{\mathbf{T}}^\mathrm{I} : \boldsymbol{\sigma}^0. \tag{39}$$

Here, $\boldsymbol{\varepsilon}^0$ and $\boldsymbol{\sigma}^0$ represent the strain and stress tensors in a homogeneous material composing only of the matrix material and are uniform tensors. $\bar{\boldsymbol{\varepsilon}}^\mathrm{I}$ and $\bar{\boldsymbol{\sigma}}^\mathrm{I}$ are the volume average strain and stress tensors in the inhomogeneity. $\bar{\mathbf{E}}^\mathrm{I}$ or $\bar{\mathbf{T}}^\mathrm{I}$ can be estimated by the GSCM scheme, in which the inhomogeneity is assumed to be embedded in a finite shell made of the matrix material, and the whole inhomogeneity-shell structure is again embedded in an infinite medium with unknown mechanical properties, as shown in Fig. 3a. The unknown mechanical properties of the infinite medium are the effective properties of the heterogeneous materials. Thus, we

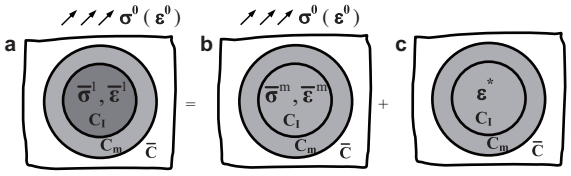

Figure 3 **a** The GSCM (three-phase) configuration for a heterogeneous material containing spherical (circular) inhomogeneities. **b**, **c** The Eshelby equivalent inclusion method in a volume average sense for the three-phase configuration. Reproduced from Ref. [130].

call the infinite medium the equivalent homogeneous medium. The matrix shell in Fig. 3a can be regarded as the interphase, and the equivalent homogeneous medium can be treated as the infinite matrix. Then, the effective stiffness tensor (or effective compliance tensor) of the heterogeneous material can be directly calculated by substituting the strain and stress concentration tensors for the inhomogeneity in the three-phase configuration into Eq. (37) or (38) [130]. The effective bulk and shear moduli of heterogeneous materials estimated by this procedure were found to be the same as those predicted by Christensen et al. [132, 150]. However, the obtained effective shear modulus is implicit in the form of a quadratic equation with redundant coefficients, which poses a challenge for solving the effective shear modulus.

We have proposed a unified micromechanical scheme for multiphase composites with interface effects [130, 151, 152]. Different from previous schemes, the strain concentration tensor $\bar{\mathbf{E}}^{\mathrm{I}}$ in this new micromechanical scheme is obtained by the Eshelby equivalent inclusion method shown in Fig. 3b and c rather than using the configuration in Fig. 3a. And the Eshelby equivalent inclusion method is in a volume average sense. In the following, a brief description of this framework is given.

Consider a three-phase configuration shown in Fig. 3a, which is under a remote stress $\boldsymbol{\sigma}^0$. The remote stress induces the stress in the inhomogeneity Ω, whose volume average form is $\bar{\boldsymbol{\sigma}}^{\mathrm{I}}$ with a bar denoting the volume average. Then, one can replace the region of inhomogeneity with the stiffness tensor of $\mathbf{C}_{\mathrm{I}}$ by the matrix material with the stiffness tensor $\mathbf{C}_{\mathrm{m}}$, as shown in Fig. 3b. The volume average stress in the replaced region is $\bar{\boldsymbol{\sigma}}^{\mathrm{m}}$ for the same remote stress $\boldsymbol{\sigma}^0$, which meets the condition $\bar{\boldsymbol{\sigma}}^{\mathrm{m}} = \mathbf{B} : \boldsymbol{\sigma}^0$. The fourth-order tensor $\mathbf{B}$ is equal to the classical stress concentration tensor $\mathbf{T}^0$ [130]. The volume average stress in the replaced region $\bar{\boldsymbol{\sigma}}^{\mathrm{m}}$ is usually different from the volume average stress in the inhomogeneity $\bar{\boldsymbol{\sigma}}^{\mathrm{I}}$. And the replaced region is further applied a uniform eigenstrain $\boldsymbol{\varepsilon}^*$, as shown in Fig. 3c. In the classical Eshelby equivalent inclusion method, the eigenstrain $\boldsymbol{\varepsilon}^*$ satisfies the following condition:

$$\mathbf{C}_{\mathrm{I}} : (\bar{\boldsymbol{\varepsilon}}^{\mathrm{m}} + \bar{\boldsymbol{\varepsilon}}') = \mathbf{C}_{\mathrm{m}} : (\bar{\boldsymbol{\varepsilon}}^{\mathrm{m}} + \bar{\boldsymbol{\varepsilon}}' - \boldsymbol{\varepsilon}^*), \tag{40}$$

where $\bar{\boldsymbol{\varepsilon}}^{\mathrm{m}}$ is the volume average strain in the replaced region. The relationship between the disturbed strain $\bar{\boldsymbol{\varepsilon}}'$ and the uniform eigenstrain $\boldsymbol{\varepsilon}^*$ is $\bar{\boldsymbol{\varepsilon}}' = \bar{\mathbf{S}}^{\mathrm{I}} : \boldsymbol{\varepsilon}^*$ with $\bar{\mathbf{S}}^{\mathrm{I}}$ being the volume average Eshelby tensor in the replaced spherical region in Fig. 3c [130].

An approximation for the stress concentration tensor $\bar{\mathbf{T}}^{\mathrm{I}}$ is given here based on the Eshelby equivalent inclusion method in a volume average sense [130], which is represented by $\bar{\mathbf{T}}^*$ and is given by

$$\bar{\mathbf{T}}^* = \left[\mathbf{I}^{(4s)} - \mathbf{C}_{\mathrm{I}} : \bar{\mathbf{S}}^{\mathrm{I}} : (\mathbf{C}_{\mathrm{I}}{}^{-1} - \mathbf{C}_{\mathrm{m}}{}^{-1})\right]^{-1} : \mathbf{C}_{\mathrm{I}} : \mathbf{C}_{\mathrm{m}}{}^{-1} : \mathbf{B}, \tag{41}$$

where $\mathbf{I}^{(4s)}$ is the fourth-order symmetric identity tensor in three-dimensional space [138]. Similarly, an approximation for the strain concentration tensor $\bar{\mathbf{E}}^{\mathrm{I}}$ represented by $\bar{\mathbf{E}}^*$ can be expressed as

$$\bar{\mathbf{E}}^* = \left[\mathbf{I}^{(4s)} - \bar{\mathbf{S}}^{\mathrm{I}} : \mathbf{C}_{\mathrm{m}}{}^{-1} : (\mathbf{C}_{\mathrm{m}} - \mathbf{C}_{\mathrm{I}})\right]^{-1} : \mathbf{A}. \tag{42}$$

The fourth-order tensor $\mathbf{A}$ satisfies the condition $\bar{\boldsymbol{\varepsilon}}^{\mathrm{m}} = \mathbf{A} : \boldsymbol{\varepsilon}^0$ and is expressed as $\mathbf{A} = \mathbf{C}_{\mathrm{I}}{}^{-1} : \mathbf{B} : \mathbf{C}_{\mathrm{m}}$.

When the spherical inhomogeneity is isotropic and is embedded in an isotropic matrix, $\bar{\mathbf{T}}^*$ can be written as

$$\bar{\mathbf{T}}^* = \alpha^* \mathbf{J}_3 + \beta^* \mathbf{K}_3, \tag{43}$$

with

$$\mathbf{J}_3 = \frac{1}{3}\mathbf{I}^{(2)} \otimes \mathbf{I}^{(2)}, \quad \mathbf{K}_3 = -\frac{1}{3}\mathbf{I}^{(2)} \otimes \mathbf{I}^{(2)} + \mathbf{I}^{(4s)}, \tag{44}$$

where α^* is the dilatational component, and β^* is the deviatoric component. It is found that α^* is equal to the exact result obtained by directly solving the problem in Fig. 3a, and β^* is identical to the exact numerical results [130]. It means that the approximation of the stress concentration tensor is of high accuracy. Therefore, we can predict the effective mechanical properties of heterogeneous materials by replacing $\bar{\mathbf{T}}^{\mathrm{I}}$ with $\bar{\mathbf{T}}^*$. Compared with the classical GSCM, the replacement method has a simpler expression for the effective shear modulus [130]. Duan et al. [130] also found that this replacement method is self-consistent. Furthermore, this replacement method described above can be applied to circular inhomogeneities, and $\bar{\mathbf{S}}^{\mathrm{I}}$, $\bar{\mathbf{T}}^{\mathrm{I}}$, and $\bar{\mathbf{T}}^*$ show similar properties to those of the spherical inhomogeneity.

When further considering a composite containing multiple different particles denoted by $k = 2, 3, \cdots, N$, we can obtain the effective stiffness tensor $\bar{\mathbf{C}}$ and compliance tensor $\bar{\mathbf{D}}$ by the following decoupled formulas:

$$\begin{aligned} \bar{\mathbf{C}} &= \mathbf{C}_{\mathrm{m}} + \sum_{k=2}^{N} f_k(\mathbf{C}_k - \mathbf{C}_{\mathrm{m}}) : \bar{\mathbf{E}}^k, \\ \bar{\mathbf{D}} &= \mathbf{D}_{\mathrm{m}} + \sum_{k=2}^{N} f_k(\mathbf{D}_k - \mathbf{D}_{\mathrm{m}}) : \bar{\mathbf{T}}^k. \end{aligned} \tag{45}$$

Here, $\bar{\mathbf{E}}^k$ and $\bar{\mathbf{T}}^k$ are given by Eqs. (41) and (42), respectively.

After briefly describing the new micromechanical scheme, the new scheme is applied to predict the effective elastic modulus of heterogeneous materials in the following.

4.1 Heterogeneous materials containing spherical particles

Let us first consider the heterogeneous material composed of a continuous matrix and randomly distributed identical spherical particles. The obtained effective bulk modulus calculated by the new scheme is expressed as

$$\bar{\kappa} = \frac{4(1-f_{\rm I})\kappa_{\rm m}\mu_{\rm m} + \kappa_{\rm I}(3\kappa_{\rm m} + 4f_{\rm I}\mu_{\rm m})}{3(1-f_{\rm I})\kappa_{\rm I} + 3f\kappa_{\rm m} + 4\mu_{\rm m}}, \tag{46}$$

which is identical to the result given by the original GSCM [132] and the MTM [133, 146]. The effective shear modulus $\bar{\mu}$ given by the new scheme is implicit and is expressed as [130]

$$A'\left(\frac{\bar{\mu}}{\mu_{\rm m}}\right)^2 + B'\left(\frac{\bar{\mu}}{\mu_{\rm m}}\right) + C' = 0, \tag{47}$$

where

$$\begin{aligned} A' =& -\left[126f_{\rm I}^{7/3} - 252f_{\rm I}^{5/3} + 50(7 - 12\nu_{\rm m} + 8\nu_{\rm m}^2)f_{\rm I}\right] \\ & \times (1-g_3) + 4(7 - 10\nu_{\rm m})N_1, \\ B' =& \left[252f_{\rm I}^{7/3} - 504f_{\rm I}^{5/3} + 150(3-\nu_{\rm m})\nu_{\rm m}f_{\rm I}\right](1-g_3) \\ & - 3(7 - 15\nu_{\rm m})N_1, \\ C' =& -\left[126f_{\rm I}^{7/3} - 252f_{\rm I}^{5/3} + 25(7-\nu_{\rm m}^2)f_{\rm I}\right](1-g_3) \\ & - (7 + 5\nu_{\rm m})N_1, \end{aligned} \tag{48}$$

in which $N_1 = -7 + 5\nu_{\rm m} - 2g_3(4 - 5\nu_{\rm m})$, $g_3 = \mu_{\rm I}/\mu_{\rm m}$ with $\nu_{\rm m}$ being the Poisson ratio of the matrix. Compared to the result given by the original GSCM, the coefficients given by the new scheme are much simpler. And the shear modulus obtained by the new scheme through Eq. (47) is numerically indistinguishable from the results given by the GSCM [130].

When considering a general composite consisting of multiple different inhomogeneities, which are denoted by $k = 2, 3, \cdots, N$, the calculated effective modulus is of high accuracy, which is given by

$$\frac{\bar{\kappa}_{\rm e}}{\kappa_{\rm m}} \cong \prod_{k=2}^{N} \frac{\bar{\kappa}}{\kappa_{\rm m}}\left(f_k, \frac{\mu_k}{\mu_{\rm m}}, \nu_k, \nu_{\rm m}\right), \tag{49}$$

and

$$\frac{\bar{\mu}_{\rm e}}{\mu_{\rm m}} \cong \prod_{k=2}^{N} \frac{\bar{\mu}}{\mu_{\rm m}}\left(f_k, \frac{\mu_k}{\mu_{\rm m}}, \nu_k, \nu_{\rm m}\right), \tag{50}$$

where $\bar{\kappa}(f_k, \mu_k/\mu_{\rm m}, \nu_k, \nu_{\rm m})$ and $\bar{\mu}(f_k, \mu_k/\mu_{\rm m}, \nu_k, \nu_{\rm m})$ are the effective bulk modulus and the effective shear modulus of the heterogeneous materials which is composed of the matrix material of the considered multiphase composite and the k-th kind of inhomogeneity, and can be calculated from Eqs. (46) and (47). Then, the effective mechanical properties of the multiphase composite can be obtained by Eqs. (49) and (50) along with Eqs. (46) and (47). Compared with the results obtained by Christensen et al. [132, 150], the effective moduli calculated by the new scheme are very accurate.

4.2 Heterogeneous materials containing cylindrical fibers

Now, we consider a heterogeneous material, which is composed of a continuous matrix and randomly distributed but aligned identical cylindrical fibers. The aligned fibers have a volume fraction of $f_{\rm I}$. The aligned fiber-reinforced material is macroscopically transversely isotropic and has five independent elastic constants. Hill [153] and Hashin [154] proposed a model for estimating the effective elastic constants of the fiber-reinforced composites, which can accurately predict the elastic constants related to the fiber direction and the bulk modulus in the plane perpendicular to the fibers. However, it can only provide bounds on the shear modulus of the fiber-reinforced composite. Based on the configuration shown in Fig. 3a in a two-dimensional sense, Christensen and Lo [132] subsequently developed the GSCM for the fiber-reinforced composites to estimate the transverse shear modulus. Therefore, the new scheme described above can be used to estimate the effective elastic modulus of the aligned fiber-reinforced heterogeneous materials. The calculated effective plane-strain bulk modulus $\bar{k}$ is expressed as

$$\bar{\kappa} = \frac{(1-f_{\rm I})\kappa_{\rm m}\mu_{\rm m} + \kappa_{\rm I}(\kappa_{\rm m} + f_{\rm I}\mu_{\rm m})}{(1-f_{\rm I})\kappa_{\rm I} + f_{\rm I}\kappa_{\rm m} + \mu_{\rm m}}, \tag{51}$$

which is identical to the results given by the classical GSCM [132]. $\kappa_{\rm m}$ and $\mu_{\rm m}$ are the plane-strain bulk modulus and shear modulus of the matrix, respectively, and $\kappa_{\rm I}$ is the plane-strain bulk modulus of the fibers. The effective transverse shear modulus $\bar{\mu}_T$ of the heterogeneous material is implicit and needs to be solved from the following quadratic equation:

$$a'\left(\frac{\bar{\mu}_T}{\mu_{\rm m}}\right)^2 + b'\left(\frac{\bar{\mu}_T}{\mu_{\rm m}}\right) + c' = 0, \tag{52}$$

where

$$\begin{aligned} a' =& [-3f_{\rm I}^3 + 6f_{\rm I}^2 - 4(4\nu_{\rm m}^2 - 6\nu_{\rm m} + 3)f_{\rm I}](1-g_2) \\ & - (3 - 4\nu_{\rm m})N_2, \\ b' =& (6f_{\rm I}^3 - 12f_{\rm I}^2 + 8\nu_{\rm m}f_{\rm I})(1-g_2) + 2(1 - 2\nu_{\rm m})N_2, \\ c' =& (-3f_{\rm I}^3 + 6f_{\rm I}^2 - 4f_{\rm I})(1-g_2) + N_2, \end{aligned} \tag{53}$$

with $N_2 = 1 + g_2(3 - 4\nu_{\rm m})$, $g_2 = \mu_{TI}/\mu_{\rm m}$. $\nu_{\rm m}$ is the Poisson ratio of the matrix, and μ_{TI} is the transverse shear modulus of the fibers. Compared with the classical GSCM, the results obtained from Eq. (52) have the same accuracy but a simpler expression.

For the case of aligned fiber-reinforced multiphase composites, the decoupled formulas for calculating the effective elastic moduli are given by [150]

$$\frac{\bar{\kappa}_{\rm e}}{\kappa_{\rm m}} \cong \prod_{k=2}^{N} \frac{\bar{\kappa}}{\kappa_{\rm m}}\left(f_k, \frac{\mu_{Tk}}{\mu_{\rm m}}, \nu_k, \nu_{\rm m}\right), \tag{54}$$

$$\frac{\bar{\mu}_{T\rm e}}{\mu_{\rm m}} \cong \prod_{k=2}^{N} \frac{\bar{\mu}_T}{\mu_{\rm m}}\left(f_k, \frac{\mu_{Tk}}{\mu_{\rm m}}, \nu_k, \nu_{\rm m}\right), \tag{55}$$

where $\bar{\kappa}_{\rm e}$ and $\bar{\mu}_{T\rm e}$ are the transverse plane-strain bulk modulus and effective transverse shear modulus of the composites. $\bar{\kappa}$ and $\bar{\mu}_T$ are the plane-strain bulk modulus and shear modulus of the heterogeneous materials, which are only composed of the matrix materials of the considered multiphase composites and the k-th kind of fiber, which can be determined by Eqs. (51) and (52). The volume fraction of the k-th kind of fiber is f_k. Therefore, combined with Eqs. (51) and (52), and Eqs. (54) and (55), the effective modulus of the multiphase fiber-reinforced composite material is calculated.

5. Formalism for effective conductivity with interface effects

Besides the widely studied elastic properties, the conductive properties of heterogeneous materials with interface effects have also attracted considerable interest among researchers [92, 93, 96, 155, 156]. To capture the conductive properties of the interface and calculate the effect of the interface on the conductivity of the heterogeneous materials, three kinds of interface models are usually applied, i.e., the LC interface model, the HC interface model, and the interphase model [120, 121]. Take the thermal conductivity problem as an example. Both LC and HC interface models in the thermal conductivity problem are the zero-thickness interface model. There is a discontinuous temperature field and continuous normal heat flux across the LC interfaces. LC interfaces are often referred to as the interfaces with the Kapitza thermal resistance [2], where the thermal resistance can be caused by the roughness or acoustic mismatch at the boundary of two media, or results from the presence of low conductive thin interphases. The effect of the LC interface on the effective conductivity of heterogeneous materials has long been studied [146, 157-167]. For example, Hasselman and Johnson [159] have extended the classical work of Maxwell and Rayleigh, and derived an effective medium approximation (EMA) for calculating the effective thermal conductivity of heterogeneous materials. A more general formulation of EMA has been subsequently developed by Nan et al. [165] for calculating the effective thermal conductivity of the heterogeneous materials containing spherical inhomogeneities. HC interface models describe the interface with a continuous temperature field and discontinuous normal heat flux across it. Such interface behavior is caused by the presence of high conductive thin interphases [111]. The effect of the HC interface on the effective conductivity of heterogeneous materials has also been extensively studied [120, 140, 163, 166, 168, 169].

Torquato and Rintoul [163] derived the rigorous bounds for the effective conductivity of heterogeneous materials with LC and HC interfaces, which contains the information of the volume fraction of the inhomogeneities and the higher-order microstructural information. Lipton [170] introduced a new parameter named "surface to volume dissipation", and pointed out that the presence of specific particles will increase the effective conductivity of the heterogeneous materials when the "surface to volume dissipation" lies above a critical value. Garboczi et al. [171] modeled the ion diffusion in concrete with the presence of HC interfaces. Lipton and Talbot [166] gave the bound of the effective conductivity for a two-phase composite under the consideration of the LC and HC interfaces. In their bound, the interface can be highly conductive or resistive, and the material properties and geometrical arrangement of the phases can be anisotropic. In a series of works by Benveniste and Miloh, various aspects related to heterogeneous materials with LC and HC interfaces have been studied. For example, Miloh and Benveniste [120] used the ellipsoidal harmonics and mean-field approximations to predict the effective conductivity of heterogeneous materials containing ellipsoidal inhomogeneities with HC interfaces. Benveniste and Miloh [172] also proposed the concept of neutral inhomogeneity in thermal conduction and investigated the presence of neutral inhomogeneity in conduction phenomena with LC and HC interfaces.

5.1 Three kinds of interface model for conductivity

Hashin and Shtrikman [173] showed that the problems for predicting the effective characteristics of heterogeneous materials, such as heat conductivity, electrical conductivity, dielectric constant, diffusivity, and magnetic permeability, are mathematically analogous. Here, we take the prediction of thermal conductivity of heterogeneous materials as an example. Let us consider an RVE of heterogeneous material with a volume of V. $\mathbf{q}(\mathbf{x})$, $\mathbf{H}(\mathbf{x})$, and $\Phi(\mathbf{x})$ denote the local heat flux, the local intensity field, and the temperature field at position $\mathbf{x}$, respectively. The basic equations for solving the local heat flux $\mathbf{q}(\mathbf{x})$ and intensity field $\mathbf{H}(\mathbf{x})$ within the RVE are given

by

$$\begin{aligned} &\nabla\cdot\mathbf{q}(\mathbf{x})=0,\quad \nabla\times\mathbf{H}(\mathbf{x})=\mathbf{0},\quad \mathbf{H}(\mathbf{x})=-\nabla\Phi(\mathbf{x}),\\ &\mathbf{q}(\mathbf{x})=\mathbf{K}(\mathbf{x})\cdot\mathbf{H}(\mathbf{x}),\quad \text{or}\quad \mathbf{H}(\mathbf{x})=\boldsymbol{\rho}(\mathbf{x})\cdot\mathbf{q}(\mathbf{x}), \end{aligned} \tag{56}$$

where $\mathbf{K}(\mathbf{x})$ and $\boldsymbol{\rho}(\mathbf{x})$ are respectively the second-order conductivity and resistivity tensors. In general, the boundary condition on the RVE boundary ∂V is one of the following two equivalent forms:

$$\Phi(\partial \mathrm{V})=-\mathbf{H}^0\cdot\mathbf{x}\qquad\text{or}\qquad \mathbf{q}(\partial \mathrm{V})=\mathbf{q}^0, \tag{57}$$

where $\mathbf{H}^0$ and $\mathbf{q}^0$ are respectively the constant intensity and heat flux. Interface conditions between the inhomogeneities and the matrix in the heterogeneous materials must also be specified in addition to Eqs. (56) and (57) to solve the local heat flux $\mathbf{q}(\mathbf{x})$ and intensity field $\mathbf{H}(\mathbf{x})$.

As mentioned before, the LC interface model, HC interface model, and interphase model are usually used in considering the interface effect. In the following, the interface conditions for these interface models are summarized.

The LC interface simulates an interface with continuous normal heat flux and discontinuous temperature field, whose interface conditions are given by

$$[q_{_n}]=0,\quad [\Phi]=-\alpha\, q_{_n}, \tag{58}$$

where $q_{_n}$ is the normal heat flux. α is the interface parameter that describes the temperature discontinuity across the interface, with $\alpha\to 0$ denoting the ideal interface, and $\alpha\to\infty$ denoting the interface of adiabatic contact.

The HC interface simulates an interface with a continuous temperature field and discontinuous heat flux, whose interface conditions are expressed as

$$[\Phi]=0,\quad [q_{_n}]=\beta\Delta_S\Phi, \tag{59}$$

where $\Delta_S\Phi$ is the surface Laplacian of Φ. β is the surface parameter that describes the discontinuity of the heat flux, with $\beta\to 0$ denoting an ideal interface, and $\beta\to\infty$ denoting the interface in contact with a medium with infinite conductivity.

The interphase model is a three-phase model consisting of inhomogeneity, matrix, and an interface of finite thickness, in which perfect bonding conditions are generally assumed at the inhomogeneity/interphase interface Γ_{Ic} and the interphase/matrix interface Γ_{cm}. Therefore, the interface conditions are given by

$$[\Phi^j]=0,\quad [q_n^j]=0,\quad j=1,2, \tag{60}$$

where superscript $j=1$ and 2 represents the interfaces Γ_{Ic} and Γ_{cm}, respectively. $[\Phi^j]$ and $[q_n^j]$ denote the temperature field discontinuity and heat flux discontinuity, respectively.

After given basic equations and interface/boundary conditions for the thermal conductivity problem, the effective conductivity of the heterogeneous materials can be obtained by the micromechanical model. In the following, a brief illustration of the micromechanical frameworks for estimating the effective conductivity of the heterogeneous materials with the interface effects is given.

5.2 Frameworks for effective conductivity

Consider a heterogeneous material with the inhomogeneity conductivity tensor $\mathbf{K}_{\mathrm{I}}$ (resistivity tensor $\boldsymbol{\rho}_{\mathrm{I}}$) and matrix conductivity tensor $\mathbf{K}_{\mathrm{m}}$ (resistivity tensor $\boldsymbol{\rho}_{\mathrm{m}}$), similar to those of the elasticity problems, the definitions of the volume average intensity and volume average heat flux in the RVE with boundary ∂V are

$$\bar{\mathbf{H}}=\frac{1}{V}\int_V\mathbf{H}\,\mathrm{d}V=-\frac{1}{V}\int_{\partial V}\Phi\ \mathbf{m}\,\mathrm{d}A, \tag{61}$$

and

$$\bar{\mathbf{q}}=\frac{1}{V}\int_V\mathbf{q}\mathrm{d}V=\frac{1}{V}\int_{\partial V}(\mathbf{q}\cdot\mathbf{m})\,\mathbf{x}\,\mathrm{d}A. \tag{62}$$

In the presence of imperfect interfaces with temperature and flux discontinuities, these averages can be written as [174]

$$\bar{\mathbf{H}}=(1-f_I)\,\bar{\mathbf{H}}^{\mathrm{m}}+f_{\mathrm{I}}\bar{\mathbf{H}}^{\mathrm{I}}+\frac{f_{\mathrm{I}}}{V_{\mathrm{I}}}\int_\Gamma[\Phi]\,\mathbf{n}\,\mathrm{d}\Gamma, \tag{63}$$

and

$$\bar{\mathbf{q}}=(1-f_{\mathrm{I}})\,\bar{\mathbf{q}}^{\mathrm{m}}+f_I\,\bar{\mathbf{q}}^{\mathrm{I}}+\frac{f_{\mathrm{I}}}{V_{\mathrm{I}}}\int_\Gamma([\mathbf{q}]\cdot\mathbf{n})\,\mathbf{x}\,\mathrm{d}\Gamma. \tag{64}$$

In Eqs. (63) and (64), $[\mathbf{q}]=\mathbf{0}$ for the LC interface model and $[\Phi]=0$ for the HC interface model.

5.2.1 *Frameworks with LC interface model*

Under $\Phi(S)=-\mathbf{H}^0\cdot\mathbf{x}$, the effective conductivity $\bar{\mathbf{K}}$ is given by [146]

$$\bar{\mathbf{K}}=\mathbf{K}_{\mathrm{m}}+f_{\mathrm{I}}\,(\mathbf{K}_{\mathrm{I}}-\mathbf{K}_{\mathrm{m}})\cdot\mathbf{M}'+f_{\mathrm{I}}\,\mathbf{K}_{\mathrm{m}}\cdot\mathbf{N}', \tag{65}$$

in which $\mathbf{M}'$ and $\mathbf{N}'$ are two intensity concentration tensors in the inhomogeneity and at the interface expressed as

$$\bar{\mathbf{H}}^{\mathrm{I}}=\mathbf{M}'\cdot\mathbf{H}^0,\quad \frac{1}{V_{\mathrm{I}}}\int_\Gamma[\Phi]\,\mathbf{n}\,\mathrm{d}\Gamma=\mathbf{N}'\cdot\mathbf{H}^0. \tag{66}$$

Under $\mathbf{q}(S)=\mathbf{q}^0$, the effective resistivity $\bar{\boldsymbol{\rho}}$ is

$$\bar{\boldsymbol{\rho}}=\boldsymbol{\rho}_{\mathrm{m}}+f_{\mathrm{I}}\,(\boldsymbol{\rho}_{\mathrm{I}}-\boldsymbol{\rho}_{\mathrm{m}})\cdot\mathbf{P}'+f_{\mathrm{I}}\,\boldsymbol{\rho}_{\mathrm{m}}\cdot\mathbf{Q}', \tag{67}$$

in which $\mathbf{P}'$ and $\mathbf{Q}'$ are two flux concentration tensors in the inhomogeneity and at the interface expressed as

$$\bar{\mathbf{q}}^{\mathrm{I}}=\mathbf{P}'\cdot\mathbf{q}^0,\quad \frac{1}{V_{\mathrm{I}}}\int_\Gamma[\Phi]\,\mathbf{n}\,\mathrm{d}\Gamma=\boldsymbol{\rho}_{\mathrm{m}}\cdot\mathbf{Q}'\cdot\mathbf{q}^0. \tag{68}$$

5.2.2 *Frameworks with HC interface model*

Under $\Phi(S) = -\mathbf{H}^0 \cdot \mathbf{x}$, the effective conductivity $\bar{\mathbf{K}}$ is

$$\bar{\mathbf{K}} = \mathbf{K}_\mathrm{m} + f_\mathrm{I}\,(\mathbf{K}_\mathrm{I} - \mathbf{K}_\mathrm{m}) \cdot \mathbf{R}' + f_\mathrm{I}\,\mathbf{K}_\mathrm{m} \cdot \mathbf{G}', \tag{69}$$

in which two intensity concentration tensors $\mathbf{R}'$ and $\mathbf{G}'$ in the inhomogeneity and at the interface are defined by

$$\bar{\mathbf{H}}^\mathrm{I} = \mathbf{R}' \cdot \mathbf{H}^0, \quad \frac{1}{V_\mathrm{I}} \int_\Gamma ([\mathbf{q}] \cdot \mathbf{n}) \otimes \mathbf{x}\, \mathrm{d}\Gamma = \mathbf{K}_\mathrm{m} \cdot \mathbf{G}' \cdot \mathbf{H}^0. \tag{70}$$

Under $\mathbf{q}(S) = \mathbf{q}^0$, the effective resistivity $\bar{\boldsymbol{\rho}}$ is

$$\bar{\boldsymbol{\rho}} = \boldsymbol{\rho}_\mathrm{m} + f_\mathrm{I}\,(\boldsymbol{\rho}_\mathrm{I} - \boldsymbol{\rho}_\mathrm{m}) \cdot \mathbf{U}' - f_\mathrm{I}\,\boldsymbol{\rho}_\mathrm{m} \cdot \mathbf{W}', \tag{71}$$

in which two strain concentration tensors $\mathbf{U}'$ and $\mathbf{W}'$ in the inhomogeneity and at the interface are defined by

$$\bar{\mathbf{q}}^\mathrm{I} = \mathbf{U}' \cdot \mathbf{q}^0, \quad \frac{1}{V_\mathrm{I}} \int_\Gamma ([\mathbf{q}] \cdot \mathbf{n}) \otimes \mathbf{x}\, \mathrm{d}\Gamma = \mathbf{W}' \cdot \mathbf{q}^0. \tag{72}$$

It is noted that Eqs. (65) and (67) for the LC interface model, and Eqs. (69) and (71) for the HC interface model can be applied to estimate the effective conductivity of heterogeneous materials through the micromechanical methods, such as the dilute concentration approximation and the GSCM [175], once the intensity and flux concentration tensors in these expressions have been obtained.

5.2.3 *Frameworks with interphase model*

When considering the interphase model, let $\mathbf{K}_\mathrm{c}$ and $\boldsymbol{\rho}_\mathrm{c}$ be the conductivity and resistivity tensors of the interphase. According to Eq. (62), the volume average intensity and flux of the RVE are then given by

$$\bar{\mathbf{H}} = f_\mathrm{m}\bar{\mathbf{H}}^\mathrm{m} + f_\mathrm{I}\bar{\mathbf{H}}^\mathrm{I} + f_\mathrm{c}\bar{\mathbf{H}}^\mathrm{c}, \tag{73}$$

and

$$\begin{aligned}\bar{\mathbf{H}} &= f_\mathrm{m}\bar{\mathbf{H}}^\mathrm{m} + f_\mathrm{I}\bar{\mathbf{H}}^\mathrm{I} + f_\mathrm{c}\bar{\mathbf{H}}^\mathrm{c}\bar{\mathbf{q}}^\mathrm{I} + f_\mathrm{c}\bar{\mathbf{q}}^\mathrm{c} \\ &= f_\mathrm{m}\mathbf{K}_\mathrm{m} \cdot \bar{\mathbf{H}}^\mathrm{m} + f_\mathrm{I}\mathbf{K}_\mathrm{I} \cdot \bar{\mathbf{H}}^\mathrm{I} + f_\mathrm{c}\mathbf{K}_c \cdot \bar{\mathbf{H}}^\mathrm{c}.\end{aligned} \tag{74}$$

Then the effective conductivity $\bar{\mathbf{K}}$ can be calculated by the following expression:

$$\bar{\mathbf{K}} \cdot \bar{\mathbf{H}} = \mathbf{K}_\mathrm{m} \cdot \bar{\mathbf{H}}^\mathrm{m} + f_\mathrm{I}\,(\mathbf{K}_\mathrm{I} - \mathbf{K}_\mathrm{m}) \cdot \bar{\mathbf{H}}^\mathrm{I} + f_\mathrm{c}\,(\mathbf{K}_\mathrm{c} - \mathbf{K}_\mathrm{m}) \cdot \bar{\mathbf{H}}^\mathrm{c}. \tag{75}$$

6. Scaling laws for size-dependent properties

Because of their importance in various fields, the size-dependent properties of materials have been studied for a long time, and have recently received more attention at the nanoscale. In nature and modern industry, nano-structures are common [69-71, 176-180] and the large surface area to volume ratio of these nano-structures significantly affects their properties. For instance, the failure mode can be changed by reducing the size of the solids. Brittle calcium carbonate particles with a size less than 850 nm will be ductile and can not be comminutied by fracturing [181, 182].

When considering the size-dependent properties of materials with the feature size of L, let $F(L)$ denote the concerned property at a small size L, and $F(\infty)$ denote the corresponding property of the bulk. Based on the dimensional analysis, the ratio of $F(L)$ to $F(\infty)$ can be then written as a function of some non-dimensional variables X_j ($j = 1, 2, \cdots, M$) and a size-related non-dimensional parameter l_in/L, i.e.,

$$\frac{F(L)}{F(\infty)} = \mathscr{F}(X_j, l_\mathrm{in}/L), \tag{76}$$

where l_in is an intrinsic length scale related to the surface properties. The function in Eq. (76) can be extended in powers of l_in/L for many physical properties. When l_in is much smaller than L, only the linear term in the extended expressions of l_in/L needs to be retained. Therefore, the size-dependent properties of the considered materials can be accurately described by the scaling laws expressed as

$$\frac{F(L)}{F(\infty)} = 1 + \mathscr{A}\frac{l_\mathrm{in}}{L}, \tag{77}$$

and

$$\frac{F(\infty)}{F(L)} = 1 + \mathscr{B}\frac{l_\mathrm{in}}{L}, \tag{78}$$

where $\mathscr{A}$ and $\mathscr{B}$ are two non-dimensional coefficients. In the following, we will confirm that the scaling laws Eqs. (77) and (78) are obeyed by many materials properties such as elastic modulus, thermal conductivity, and melting temperature.

6.1 Scaling laws for size-dependent elasticity

When considering the interface effects on the effective elastic properties through LSM and ISM, some intrinsic length scales emerge, i.e.,

$$l_r = \frac{\mu_\mathrm{m}}{\beta_n}, \quad l_\theta = \frac{\mu_\mathrm{m}}{\beta_s}, \quad \text{for LSM}, \tag{79}$$

and

$$l_\lambda = \frac{\lambda_s}{\mu_\mathrm{m}}, \quad l_\mu = \frac{\mu_s}{\mu_\mathrm{m}}, \quad \text{for ISM}. \tag{80}$$

Therefore, the effective modulus of heterogeneous materials with the LSM or ISM interface effects are usually size-dependent. The detailed size dependence of the effective modulus of the heterogeneous materials can be investigated by the micromechanical schemes described above. When the length scale of the inhomogeneity is much smaller than

the characteristic size of the heterogeneous material, the size dependence can be briefly described by two simple scaling laws, which are very accurate.

For illustrative purposes, a two-phase heterogeneous material is considered here. The ISM interface model is first studied which describes the elasticity of the isotropic interface with two surface elastic constants λ_s and μ_s [89, 183], which results in two intrinsic length scales l_λ and l_μ [32, 83]. Then, the mechanical properties of the heterogeneous material are expected to obey a scaling law [184], which is given by

$$\frac{F(L)}{F(\infty)} = 1 + \frac{1}{L}(\alpha_\lambda l_\lambda + \beta_\mu l_\mu). \tag{81}$$

The scaling law is a linear combination of two length scales with α_λ and β_μ being the coefficients. Equation (81) can be applied to many properties, such as the maximum stress concentration factor, the effective elastic modulus, the Eshelby tensor, and the effective thermal expansion coefficient.

The melting point temperature of nanomaterials also shows size dependence, which is supported by a large amount of test data and theoretical models [185-192]. It has been shown that the melting temperature $T(R)$ of a spherical nanoparticle depends on the particle radius R and the corresponding scaling law is given by

$$\frac{T(R)}{T(\infty)} = 1 - 2\frac{l_{\text{in}}}{R}. \tag{82}$$

The intrinsic length scale l_{in} is given by Wang et al. [184]. Equation (82) is the Gibbs-Thomson equation, which takes account of the relative thermodynamic contributions of surface and bulk energy and provides theoretical support for the scaling law Eq. (77). The size-dependent evaporation temperature of nanoparticles has also been confirmed to follow the scaling law Eq. (77) [193].

Besides the ISM interface, the LSM interface has also been widely used to simulate the interface properties of heterogeneous materials. For a two-phase heterogeneous material, the effective elastic modulus can be described by a simple scaling law, which is expressed as [152]

$$\frac{F(\infty)}{F(L)} = 1 + \frac{1}{L}(\alpha_r l_r + \beta_\theta l_\theta), \tag{83}$$

where α_r and β_θ are the coefficients to combine two length scales l_r and l_θ.

6.2 Scaling laws for size-dependent conductivity

As mentioned above, HC and LC interface models are the widely used interface models to estimate the effective conductivity of heterogeneous materials with two intrinsic length scales emerged in the derivation of the effective conductivity tensors, i.e.,

$$l_{\text{low}} = \alpha K_{\text{m}}, \quad \text{for LC interface model,} \tag{84}$$

and

$$l_{\text{high}} = \frac{\beta}{K_{\text{m}}}, \quad \text{for HC interface model,} \tag{85}$$

where K_{m} is the conductivity of the matrix. The scaling law for a heterogeneous material composed of spherical inhomogeneities and continuous matrix with the LC interface is given by

$$\frac{\bar{K}(\infty)}{\bar{K}(R)} = 1 + \frac{1}{R}\Upsilon_{ls} l_{\text{low}}, \tag{86}$$

where Υ_{ls} is a non-dimensional parameter, and is given by

$$\Upsilon_{ls} = \frac{9f\Lambda_2^2}{[(1+2f)\Lambda_2 + 2(1-f)][(1-f)\Lambda_2 + 2 + f]}. \tag{87}$$

The size-dependent scaling law of the effective conductivity of the heterogeneous material with the HC interface is given by

$$\frac{\bar{K}(R)}{\bar{K}(\infty)} = 1 + \frac{1}{R}\Upsilon_{hs} l_{\text{high}}. \tag{88}$$

Here, Υ_{hs} is a non-dimensional parameter. It is interesting that, since the interface properties modeled by the ISM (or HC) interface model and LSM (or LC) interface model have opposite physical interpretations, the corresponding scaling laws, namely, Eqs. (81) and (83), Eqs. (86) and (88), are formally mathematically reciprocal.

It has been confirmed that the size dependence of the material properties can be accurately depicted by the scaling law formulated by Eq. (77) or (78). In addition, the scaling law can also help to examine the material properties obtained by experimental and numerical methods, and can help to reduce the large number of experiments and simulations used to determine the parameter $\mathscr{A} l_{\text{in}}$ or $\mathscr{B} l_{\text{in}}$. Since experiments at nano-scale usually require specific instruments and elaborate analysis, such as the experiments on compounds, alloys [194], and nano-particles [195], reducing the number of experiments through the scaling law is quite important and useful in analyzing the properties of nanostructured materials.

7. Concluding remarks

In summary, this paper reviews the fundamental issues in studying the elastic and conductive properties of heterogeneous materials under the consideration of interface effects, including the interface models, Eshelby formalism, and micromechanical frameworks for elastic and conductive properties. These results demonstrate that the interface between the

inhomogeneities and the matrix greatly affects the elastic and conductive properties of nano-structured materials. Furthermore, scaling laws for the elastic and conductive problems with the interface effects are also reviewed to show the influence of the characterized size of the nano-structured and how elastic and conductive properties vary with the characterized sizes.

It should be emphasized that this work focuses on the interface effects on the linear properties (such as the elastic moduli and conductivity), which have been well developed. In contrast, interface influence on the finite deformation and nonlinear elastic response has obtained less attention and few results. Studying the nonlinear mechanical behavior is important for characterizing soft materials and biomaterials. Thus, the influence of the interface on the nonlinear behavior of the composites needs more attention and further investigation in the future.

This work was supported by the National Natural Science Foundation of China (Grant Nos. 11988102, 11872004, and 91848201).

1 Y. M. Shabana, B. L. Karihaloo, H. X. Zhu, and S. Kulasegaram, Influence of processing defects on the measured properties of Cu-Al_2O_3 composites: A forensic investigation, Compos. Part A-Appl. Sci. Manuf. **46**, 140 (2013).
2 P. L. Kapitza, Collected Papers of P. L. Kapitza, editor by D. ter Haar, Vol. 2, Pergamon, (Reprinted 1965) (1941), p. 581.
3 G. Chatzigeorgiou, F. Meraghni, and A. Javili, Generalized interfacial energy and size effects in composites, J. Mech. Phys. Solids **106**, 257 (2017).
4 H. L. Duan, J. Wang, and B. L. Karihaloo, Theory of elasticity at the nanoscale, Adv. Appl. Mech. **42**, 1 (2009).
5 Z. Y. Ong, Thickness-dependent Kapitza resistance in multilayered graphene and other two-dimensional crystals, Phys. Rev. B **95**, 155309 (2017), arXiv: 1704.00435.
6 B. He, B. Mortazavi, X. Zhuang, and T. Rabczuk, Modeling Kapitza resistance of two-phase composite material, Composite Struct. **152**, 939 (2016).
7 D. H. Hurley, M. Khafizov, and S. L. Shinde, Measurement of the Kapitza resistance across a bicrystal interface, J. Appl. Phys. **109**, 083504 (2011).
8 S. G. Mogilevskaya, S. L. Crouch, and H. K. Stolarski, Multiple interacting circular nano-inhomogeneities with surface/interface effects, J. Mech. Phys. Solids **56**, 2298 (2008).
9 Y. Zhu, and J. Woody Ju, Interface energy effect on effective elastic moduli of spheroidal particle-reinforced nanocomposites, Acta Mech. **231**, 2697 (2020).
10 F. Mancarella, R. W. Style, and J. S. Wettlaufer, Interfacial tension and a three-phase generalized self-consistent theory of non-dilute soft composite solids, Soft Matter **12**, 2744 (2016), arXiv: 1512.07633.
11 C. W. Nan, Physics of inhomogeneous inorganic materials, Prog. Mater. Sci. **37**, 1 (1993).
12 Z. Hashin, Analysis of composite materials: A survey, J. Appl. Mech. **50**, 481 (1983).
13 S. Torquato, Random heterogeneous media: Microstructure and improved bounds on effective properties, Appl. Mech. Rev. **44**, 37 (1991).
14 P. S. Theocaris, The Mesophase Concept in Composites (Springer-verlag, Berlin, 1987).
15 P. Barai, and G. J. Weng, Mechanics of very fine-grained nanocrystalline materials with contributions from grain interior, GB zone, and grain-boundary sliding, Int. J. Plast. **25**, 2410 (2009).
16 N. Q. Chinh, P. Szommer, Z. Horita, and T. G. Langdon, Experimental evidence for grain-boundary sliding in ultrafine-grained aluminum processed by severe plastic deformation, Adv. Mater. **18**, 34 (2006).
17 J. Y. Zhang, G. Liu, and J. Sun, Strain rate effects on the mechanical response in multi- and single-crystalline Cu micropillars: Grain boundary effects, Int. J. Plast. **50**, 1 (2013).
18 X. Zhu, Z. Yang, X. Guo, and W. Chen, Modulus prediction of asphalt concrete with imperfect bonding between aggregate-asphalt mastic, Compos. Part B-Eng. **42**, 1404 (2011).
19 Y. Zhang, J. W. Ju, H. Zhu, and Z. Yan, A novel multi-scale model for predicting the thermal damage of hybrid fiber-reinforced concrete, Int. J. Damage Mech. **29**, 19 (2020).
20 K. Yanase, and J. W. Ju, Overall elastoplastic damage responses of spherical particle-reinforced composites containing imperfect interfaces, Int. J. Damage Mech. **23**, 411 (2014).
21 T. Mura, and R. Furuhashi, The elastic inclusion with a sliding interface, J. Appl. Mech. **51**, 308 (1984).
22 Y. J. Wei, and L. Anand, Grain-boundary sliding and separation in polycrystalline metals: Application to nanocrystalline fcc metals, J. Mech. Phys. Solids **52**, 2587 (2004).
23 M. A. Linne, T. R. Bieler, and S. Daly, The effect of microstructure on the relationship between grain boundary sliding and slip transmission in high purity aluminum, Int. J. Plast. **135**, 102818 (2020).
24 J. Schiøtz, F. D. Di Tolla, and K. W. Jacobsen, Softening of nanocrystalline metals at very small grain sizes, Nature **391**, 561 (1998).
25 T. Y. Zhang, and J. E. Hack, On the elastic stiffness of grain boundaries, Phys. Stat. Sol. (a) **131**, 437 (1992).
26 L. J. Walpole, A coated inclusion in an elastic medium, Mathematical Proceedings of the Cambridge Philosophical Society, Cambridge University Press **83**, 495 (1978).
27 B. L. Karihaloo, and K. Viswanathan, A partially debonded ellipsoidal inclusion in an elastic medium. Part I: Stress and displacement fields, Mech. Mater. **7**, 191 (1988).
28 B. L. Karihaloo, and K. Viswanathan, A partially debonded ellipsoidal inclusion in an elastic medium. Part II: Stress intensity factors and debond opening displacement, Mech. Mater. **7**, 199 (1988).
29 Z. Hashin, The spherical inclusion with imperfect interface, J. Appl. Mech. **58**, 444 (1991).
30 J. Qu, The effect of slightly weakened interfaces on the overall elastic properties of composite materials, Mech. Mater. **14**, 269 (1993).
31 Z. Zhong, and S. A. Meguid, J. Elasticity **46**, 91 (1997).
32 H. L. Duan, J. Wang, Z. P. Huang, and Y. Zhong, Stress fields of a spheroidal inhomogeneity with an interphase in an infinite medium under remote loadings, Proc. R. Soc. A **461**, 1055 (2005).
33 B. Idzikowski, S. Mielcarek, P. Misiuna, Z. Śniadecki, and A. C. Brańka, Mechanical properties of amorphous and partially crystallized $Y_{50}Cu_{42}Al_8$ alloys, Intermetallics **21**, 75 (2012).
34 S. Krichen, L. Liu, and P. Sharma, Liquid inclusions in soft materials: Capillary effect, mechanical stiffening and enhanced electromechanical response, J. Mech. Phys. Solids **127**, 332 (2019).
35 R. W. Style, R. Boltyanskiy, B. Allen, K. E. Jensen, H. P. Foote, J. S. Wettlaufer, and E. R. Dufresne, Stiffening solids with liquid inclusions, Nat. Phys. **11**, 82 (2015), arXiv: 1407.6424.
36 A. Y. Zemlyanova, and S. G. Mogilevskaya, On spherical inhomogeneity with Steigmann-Ogden interface, J. Appl. Mech. **85**, 121009 (2018).
37 J. Wang, P. Yan, L. Dong, and S. N. Atluri, Spherical nano-inhomogeneity with the Steigmann-Ogden interface model under general uniform far-field stress loading, Int. J. Solids Struct. **185-186**, 311 (2020).
38 T. Chen, G. J. Dvorak, and C. C. Yu, Solids containing spherical nano-inclusions with interface stresses: Effective properties and thermal-mechanical connections, Int. J. Solids Struct. **44**, 941 (2007).
39 S. Brisard, L. Dormieux, and D. Kondo, Hashin-Shtrikman bounds on the bulk modulus of a nanocomposite with spherical inclusions and

interface effects, Comput. Mater. Sci. **48**, 589 (2010).
40 H. L. Quang, and Q. C. He, Variational principles and bounds for elastic inhomogeneous materials with coherent imperfect interfaces, Mech. Mater. **40**, 865 (2008).
41 X. Haller, Y. Monerie, S. Pagano, and P. G. Vincent, Elastic behavior of porous media with spherical nanovoids, Int. J. Solids Struct. **84**, 99 (2016).
42 B. Paliwal, and M. Cherkaoui, Estimation of anisotropic elastic properties of nanocomposites using atomistic-continuum interphase model, Int. J. Solids Struct. **49**, 2424 (2016).
43 A. Gharahi, and P. Schiavone, Effective elastic properties of plane micropolar nano-composites with interface flexural effects, Int. J. Mech. Sci. **149**, 84 (2018).
44 S. T. Gu, Q. C. He, and V. Pensée, Homogenization of fibrous piezoelectric composites with general imperfect interfaces under anti-plane mechanical and in-plane electrical loadings, Mech. Mater. **88**, 12 (2015).
45 T. Chen, G. J. Dvorak, and C. C. Yu, Solids containing spherical nano-inclusions with interface stresses: Effective properties and thermal-mechanical connections, Int. J. Solids Struct. **44**, 941 (2007).
46 T. Chen, G. J. Dvorak, and C. C. Yu, Size-dependent elastic properties of unidirectional nano-composites with interface stresses, Acta Mech. **188**, 39 (2007).
47 Z. Wang, J. Zhu, X. Y. Jin, W. Q. Chen, and C. Zhang, Effective moduli of ellipsoidal particle reinforced piezoelectric composites with imperfect interfaces, J. Mech. Phys. Solids **65**, 138 (2014).
48 B. Jiang, and G. J. Weng, A generalized self-consistent polycrystal model for the yield strength of nanocrystalline materials, J. Mech. Phys. Solids **52**, 1125 (2004).
49 H. Tan, Y. Huang, C. Liu, and P. H. Geubelle, The Mori-Tanaka method for composite materials with nonlinear interface debonding, Int. J. Plast. **21**, 1890 (2005).
50 H. Tan, C. Liu, Y. Huang, and P. H. Geubelle, The cohesive law for the particle/matrix interfaces in high explosives, J. Mech. Phys. Solids **53**, 1892 (2005).
51 H. Gleiter, Nanostructured materials: Basic concepts and microstructure, Acta Mater. **48**, 1 (2000).
52 S. Brach, L. Dormieux, D. Kondo, and G. Vairo, Strength properties of nanoporous materials: A 3-layered based non-linear homogenization approach with interface effects, Int. J. Eng. Sci. **115**, 28 (2017).
53 T. Goudarzi, R. Avazmohammadi, and R. Naghdabadi, Surface energy effects on the yield strength of nanoporous materials containing nanoscale cylindrical voids, Mech. Mater. **42**, 852 (2010).
54 P. L. Palla, S. Giordano, and L. Colombo, Lattice model describing scale effects in nonlinear elasticity of nanoinhomogeneities, Phys. Rev. B **81**, 214113 (2010), arXiv: 1006.2708.
55 F. D. Fischer, and J. Svoboda, Stresses in hollow nanoparticles, Int. J. Solids Struct. **47**, 2799 (2010).
56 H. Gleiter, T. Schimmel, and H. Hahn, Nanostructured solids—From nano-glasses to quantum transistors, Nano Today **9**, 17 (2014).
57 L. Colombo, and S. Giordano, Nonlinear elasticity in nanostructured materials, Rep. Prog. Phys. **74**, 116501 (2011).
58 R. Shuttleworth, The surface tension of solids, Proc. Phys. Soc. A **63**, 444 (1950).
59 C. Herring, The use of classical macroscopic concepts in surface energy problems. In: Structure and Properties of Solid Surfaces, edited by R. Gomer and C. S. Smith (The University of Chicago Press, Chicago, 1953), pp. 5-81
60 E. Orowan, Surface energy and surface tension in solids and liquids, Proc. R. Soc. Lond. A **316**, 47 (1970).
61 L. E. Murr, Interfacial Phenomena in Metals and Alloys (Addison-Wesley, London, 1975).
62 J. W. Cahn, Thermodynamics of solid and fluidsurfaces. In: Interfacial Segregation, edited by W. C. Johnson and J. M. Blakely (Americal Society for Metals, Metals Park, Ohio, 1978), pp. 3-23.
63 R. C. Cammarata, Surface and interface stresses effects in thin films, Prog. Surf. Sci. **46**, 1 (1994).
64 H. Ibach, The role of surface stress in reconstruction, epitaxial growth and stabilization of mesoscopic structures, Surf. Sci. Rep. **29**, 195 (1997).
65 P. Muller, and A. Saúl, Elastic effects on surface physics, Surf. Sci. Rep. **54**, 157 (2004).
66 W. D. Nix, and H. Gao, An atomistic interpretation of interface stress, Scripta Mater. **39**, 1653 (1998).
67 M. E. Gurtin, J. Weissmüller, and F. Larché, A general theory of curved deformable interfaces in solids at equilibrium, Philos. Mag. A **78**, 1093 (1998).
68 C. Rottman, Landau theory of coherent interphase interfaces, Phys. Rev. B **38**, 12031 (1988).
69 F. H. Streitz, R. C. Cammarata, and K. Sieradzki, Surface-stress effects on elastic properties. I. Thin metal films, Phys. Rev. B **49**, 10699 (1994).
70 F. H. Streitz, R. C. Cammarata, and K. Sieradzki, Surface-stress effects on elastic properties. II. Metallic multilayers, Phys. Rev. B **49**, 10707 (1994).
71 R. E. Miller, and V. B. Shenoy, Size-dependent elastic properties of nanosized structural elements, Nanotechnology **11**, 139 (2000).
72 Q. Ren, and Y. P. Zhao, Influence of surface stress on frequency of microcantilever-based biosensors, Microsyst. Technol. **10**, 307 (2004).
73 Y. Zhang, Q. Ren, and Y. Zhao, Modelling analysis of surface stress on a rectangular cantilever beam, J. Phys. D-Appl. Phys. **37**, 2140 (2004).
74 G. Y. Jing, H. L. Duan, X. M. Sun, Z. S. Zhang, J. Xu, Y. D. Li, J. X. Wang, and D. P. Yu, Surface effects on elastic properties of silver nanowires: Contact atomic-force microscopy, Phys. Rev. B **73**, 235409 (2006).
75 M. X. Shi, B. Liu, Z. Q. Zhang, Y. W. Zhang, and H. J. Gao, Direct influence of residual stress on the bending stiffness of cantilever beams, Proc. R. Soc. A. **468**, 2595 (2012).
76 O. Ergincan, and G. Palasantzas, Influence of random roughness on cantilever resonance frequency, Phys. Rev. B **82**, 155438 (2010).
77 Q. Deng, D. H. Gosslar, M. Smetanin, and J. Weissmüller, Electrocapillary coupling at rough surfaces, Phys. Chem. Chem. Phys. **17**, 11725 (2015).
78 Y. Chen, Q. Gao, Y. Wang, X. An, X. Liao, Y. W. Mai, H. H. Tan, J. Zou, S. P. Ringer, and C. Jagadish, Determination of Young's modulus of ultrathin nanomaterials, Nano Lett. **15**, 5279 (2015).
79 L. G. Zhou, and H. Huang, Are surfaces elastically softer or stiffer? Appl. Phys. Lett. **84**, 1940 (2004).
80 M. E. Gurtin, and A. Ian Murdoch, A continuum theory of elastic material surfaces, Arch. Rational Mech. Anal. **57**, 291 (1975).
81 D. J. Bottomley, and T. Ogino, Alternative to the Shuttleworth formulation of solid surface stress, Phys. Rev. B **63**, 165412 (2001).
82 V. B. Shenoy, Atomistic calculations of elastic properties of metallic fcc crystal surfaces, Phys. Rev. B **71**, 094104 (2005).
83 H. L. Duan, J. Wang, Z. P. Huang, and B. L. Karihaloo, Size-dependent effective elastic constants of solids containing nano-inhomogeneities with interface stress, J. Mech. Phys. Solids **53**, 1574 (2005).
84 D. J. Steigmann, and R. W. Ogden, Elastic surface-substrate interactions, Proc. R. Soc. Lond. A **455**, 437 (1999).
85 J. D. Eshelby, The determination of the elastic field of an ellipsoidal inclusion and related problems, Proc. R. Soc. Lond. A **241**, 376 (1957).
86 J. D. Eshelby, The elastic field outside an ellipsoidal inclusion, Proc. R. Soc. Lond. A **252**, 561 (1959).
87 J. D. Eshelby, The continuum theory of lattice defects, Solid State Phys. **3**, 79 (1956).
88 T. Mura, Isotropic inclusions. In: Micromechanics of Defects in Solids (Springer, Dordrecht, 1987), pp. 74-128.
89 P. Sharma, S. Ganti, and N. Bhate, Effect of surfaces on the size-dependent elastic state of nano-inhomogeneities, Appl. Phys. Lett. **82**, 535 (2003).
90 P. Sharma, and S. Ganti, Size-dependent Eshelby's tensor for embedded nano-inclusions incorporating surface/interface energies, J. Appl. Mech. **71**, 663 (2004).

91 H. L. Duan, J. Wang, B. L. Karihaloo, and Z. P. Huang, Nanoporous materials can be made stiffer than non-porous counterparts by surface modification, Acta Mater. **54**, 2983 (2006).

92 Y. Wang, G. J. Weng, S. A. Meguid, and A. M. Hamouda, A continuum model with a percolation threshold and tunneling-assisted interfacial conductivity for carbon nanotube-based nanocomposites, J. Appl. Phys. **115**, 193706 (2014).

93 J. F. Barthélémy, and F. Bignonnet, The Eshelby problem of the confocal N-layer spheroid with imperfect interfaces and the notion of equivalent particle in thermal conduction, Int. J. Eng. Sci. **150**, 103274 (2020).

94 T. Chen, and G. J. Dvorak, Fibrous nanocomposites with interface stress: Hill's and Levin's connections for effective moduli, Appl. Phys. Lett. **88**, 211912 (2006).

95 L. H. He, Self-strain of solids with spherical nanovoids, Appl. Phys. Lett. **88**, 151909 (2006).

96 H. L. Duan, and B. L. Karihaloo, Thermoelastic problem in heterogeneous materials with imperfect interfaces: Generalized Levin's formula and Hill's connections, J. Mech. Phys. Solids **55**, 1036 (2007).

97 W. Gao, S. Yu, and G. Huang, Finite element characterization of the size-dependent mechanical behaviour in nanosystems, Nanotechnology **17**, 1118 (2006).

98 Q. H. Fang, and Y. W. Liu, Size-dependent interaction between an edge dislocation and a nanoscale inhomogeneity with interface effects, Acta Mater. **54**, 4213 (2006).

99 C. Mi, and D. Kouris, Nanoparticles under the influence of surface/interface elasticity, J. Mech. Mater. Struct. **1**, 763 (2006).

100 Y. Z. Povstenko, Theoretical investigation of phenomena caused by heterogeneous surface tension in solids, J. Mech. Phys. Solids **41**, 1499 (1993).

101 J. Wang, H. L. Duan, Z. Zhang, and Z. P. Huang, An anti-interpenetration model and connections between interphase and interface models in particle-reinforced composites, Int. J. Mech. Sci. **47**, 701 (2005).

102 H. L. Duan, Y. Jiao, X. Yi, Z. P. Huang, and J. Wang, Solutions of inhomogeneity problems with graded shells and application to core-shell nanoparticles and composites, J. Mech. Phys. Solids **54**, 1401 (2006).

103 W. Xu, Y. Wu, and X. Gou, Effective elastic moduli of nonspherical particle-reinforced composites with inhomogeneous interphase considering graded evolutions of elastic modulus and porosity, Comput. Methods Appl. Mech. Eng. **350**, 535 (2019).

104 Z. Hashin, and B. W. Rosen, The elastic moduli of fiber-reinforced materials, J. Appl. Mech. **31**, 223 (1964).

105 M. P. Lutz, and R. W. Zimmerman, Effect of the interphase zone on the bulk modulus of a particulate composite, J. Appl. Mech. **63**, 855 (1996).

106 G. F. Wang, X. Q. Feng, S. W. Yu, and C. W. Nan, Interface effects on effective elastic moduli of nanocrystalline materials, Mater. Sci. Eng.-A **363**, 1 (2003).

107 Z. Hashin, Thermoelastic properties of fiber composites with imperfect interface, Mech. Mater. **8**, 333 (1990).

108 J. C. Simo, F. Armero, and R. L. Taylor, Improved versions of assumed enhanced strain tri-linear elements for 3D finite deformation problems, Comput. Methods Appl. Mech. Eng. **110**, 359 (1993).

109 M. B. Rubin, and Y. Benveniste, A Cosserat shell model for interphases in elastic media, J. Mech. Phys. Solids **52**, 1023 (2004).

110 E. Sanchez-Palencia, Comportement limite d'un probleme de transmission a travers une plaque faiblement conductrice, C. R. Acad. Sci. Paris Ser. A **270**, 1026 (1970).

111 H. P. Huy, and E. Sanchez-Palencia, Phénoménes de transmission á travers des couches minces de conductivitéélevée, J. Math. Anal. Appl. **47**, 284 (1974).

112 A. K. Mal, and S. K. Bose, Dynamic elastic moduli of a suspension of imperfectly bonded spheres, Math. Proc. Camb. Phil. Soc. **76**, 587 (1975).

113 A. Klarbring, and A. B. Movchan, Asymptotic modelling of adhesive joints, Mech. Mater. **28**, 137 (1998).

114 A. B. Movchan, Imperfect interfaces and discrete lattice structures, J. Eng. Mater. Tech. **125**, 7 (2003).

115 Y. Benveniste, and T. Miloh, Imperfect soft and stiff interfaces in two-dimensional elasticity, Mech. Mater. **33**, 309 (2001).

116 Z. Hashin, Thin interphase/imperfect interface in elasticity with application to coated fiber composites, J. Mech. Phys. Solids **50**, 2509 (2002).

117 Y. Benveniste, A general interface model for a three-dimensional curved thin anisotropic interphase between two anisotropic media, J. Mech. Phys. Solids **54**, 708 (2006).

118 P. Bövik, and P. Olsson, Effective boundary conditions for the scattering of two-dimensional SH waves from a curved thin elastic layer, Proc. R. Soc. Lond. A **439**, 257 (1992).

119 P. Bövik, On the modelling of thin interface layers in elastic and acoustic scattering problems, Q. J. Mech. Appl. Math. **47**, 17 (1994).

120 T. Miloh, and Y. Benveniste, On the effective conductivity of composites with ellipsoidal inhomogeneities and highly conducting interfaces, Proc. R. Soc. Lond. A **455**, 2687 (1999).

121 Z. Hashin, Thin interphase/imperfect interface in conduction, J. Appl. Phys. **89**, 2261 (2001).

122 H. L. Duan, B. L. Karihaloo, J. Wang, and X. Yi, Strain distributions in nano-onions with uniform and non-uniform compositions, Nanotechnology **17**, 3380 (2006).

123 H. L. Duan, B. L. Karihaloo, J. Wang, and X. Yi, Compatible composition profiles and critical sizes of alloyed quantum dots, Phys. Rev. B **74**, 195328 (2006).

124 S. Baranova, S. G. Mogilevskaya, T. H. Nguyen, and D. Schillinger, Higher-order imperfect interface modeling via complex variables based asymptotic analysis, Int. J. Eng. Sci. **157**, 103399 (2020).

125 Y. Benveniste, An $O(h^N)$ interface model of a three-dimensional curved interphase in conduction phenomena, Proc. R. Soc. A. **462**, 1593 (2006).

126 Y. Benveniste, and O. Berdichevsky, On two models of arbitrarily curved three-dimensional thin interphases in elasticity, Int. J. Solids Struct. **47**, 1899 (2010).

127 R. Rizzoni, S. Dumont, F. Lebon, and E. Sacco, Higher order model for soft and hard elastic interfaces, Int. J. Solids Struct. **51**, 4137 (2014).

128 S. Saeb, S. Firooz, P. Steinmann, and A. Javili, Generalized interfaces via weighted averages for application to graded interphases at large deformations, J. Mech. Phys. Solids **149**, 104234 (2021), arXiv: 2011.01841.

129 L. J. Walpole, Elastic behaviour of composite materials: Theoretical foundations, Adv. Appl. Mech. **21**, 169 (1981).

130 H. L. Duan, Y. Jiao, X. Yi, Z. P. Huang, and J. Wang, Solutions of inhomogeneity problems with graded shells and application to core-shell nanoparticles and composites, J. Mech. Phys. Solids **54**, 1401 (2006).

131 Y. Benveniste, The effective mechanical behaviour of composite materials with imperfect contact between the constituents, Mech. Mater. **4**, 197 (1985).

132 R. M. Christensen, and K. H. Lo, Solutions for effective shear properties in three phase sphere and cylinder models, J. Mech. Phys. Solids **27**, 315 (1979).

133 T. Mori, and K. Tanaka, Average stress in matrix and average elastic energy of materials with misfitting inclusions, Acta Metall. **21**, 571 (1973).

134 Y. P. Qiu, and G. J. Weng, Elastic moduli of thickly coated particle and fiber-reinforced composites, J. Appl. Mech. **58**, 388 (1991).

135 Z. Hashin, and P. J. M. Monteiro, An inverse method to determine the elastic properties of the interphase between the aggregate and the cement paste, Cement Concrete Res. **32**, 1291 (2002).

136 J. Aboudi, Mechanics of Composite Materials: A Unified Micromechanical Approach (Elsevier, 1991).

137 M. Bornert, C. Stolz, and A. Zaoui, Morphologically representative pattern-based bounding in elasticity, J. Mech. Phys. Solids **44**, 307 (1996).

138 S. Nemat-Nasser, and M. Hori, Micromechanics: Overall Properties

of Heterogeneous Elastic Solids, 2nd ed. (North-Holland, Amsterdam, 1999).
139 S. Torquato, Random Heterogeneous Materials: Microstructure and Macroscopic Properties (Springer-Verlag, New York, 2002).
140 G. W. Milton, The Theory of Composites (Cambridge University Press, Cambridge, 2002).
141 D. R. S. Talbot, and J. R. Willis, Variational principles for inhomogeneous non-linear media, IMA J. Appl. Math. **35**, 39 (1985).
142 P. Ponte Castañeda, and P. Suquet, Nonlinear composites, Adv. Appl. Mech. **34**, 171 (1998).
143 J. R. Willis, The overall response of nonlinear composite media, Eur. J. Mech. A-Solids **19**, S165 (2000).
144 J. Segurado, and J. Llorca, A numerical approximation to the elastic properties of sphere-reinforced composites, J. Mech. Phys. Solids **50**, 2107 (2002).
145 S. Torquato, Effective stiffness tensor of composite media: II. Applications to isotropic dispersions, J. Mech. Phys. Solids **46**, 1411 (1998).
146 Y. Benveniste, A new approach to the application of Mori-Tanaka's theory in composite materials, Mech. Mater. **6**, 147 (1987).
147 H. Ma, G. Hu, and Z. Huang, A micromechanical method for particulate composites with finite particle concentration, Mech. Mater. **36**, 359 (2004).
148 Q. S. Zheng, and D. X. Du, An explicit and universally applicable estimate for the effective properties of multiphase composites which accounts for inclusion distribution, J. Mech. Phys. Solids **49**, 2765 (2001).
149 R. Hill, Elastic properties of reinforced solids: Some theoretical principles, J. Mech. Phys. Solids **11**, 357 (1963).
150 Y. Huang, K. X. Hu, X. Wei, and A. Chandra, A generalized self-consistent mechanics method for composite materials with multiphase inclusions, J. Mech. Phys. Solids **42**, 491 (1994).
151 H. L. Duan, X. Yi, Z. P. Huang, and J. Wang, A unified scheme for prediction of effective moduli of multiphase composites with interface effects. Part I: Theoretical framework, Mech. Mater. **39**, 81 (2007).
152 H. L. Duan, X. Yi, Z. P. Huang, and J. Wang, A unified scheme for prediction of effective moduli of multiphase composites with interface effects. Part II: Application and scaling laws, Mech. Mater. **39**, 94 (2007).
153 R. Hill, Theory of mechanical properties of fibre-strengthened materials: I. Elastic behaviour, J. Mech. Phys. Solids **12**, 199 (1964).
154 Z. Hashin, Viscoelastic fiber reinforced materials, AIAA J. **4**, 1411 (1966).
155 H. L. Duan, B. L. Karihaloo, X. Yi, and J. Wang, Conductivities of heterogeneous media with graded anisotropic constituents, J. Appl. Phys. **100**, 034906 (2006).
156 H. L. Duan, B. L. Karihaloo, J. Wang, and X. Yi, Effective conductivities of heterogeneous media containing multiple inclusions with various spatial distributions, Phys. Rev. B **73**, 174203 (2006).
157 K. W. Garrett, and H. M. Rosenberg, The thermal conductivity of epoxy-resin/powder composite materials, J. Phys. D-Appl. Phys. **7**, 1247 (1974).
158 F. F. T. de Araujo, and H. M. Rosenberg, Switching behaviour and DC electrical conductivity of epoxy-resin/metal-powder composites, J. Phys. D-Appl. Phys. **9**, 1025 (1976).
159 D. P. H. Hasselman, and L. F. Johnson, Effective thermal conductivity of composites with interfacial thermal barrier resistance, J. Composite Mater. **21**, 508 (1987).
160 A. G. Every, Y. Tzou, D. P. H. Hasselman, and R. Raj, The effect of particle size on the thermal conductivity of ZnS/diamond composites, Acta Metall. Mater. **40**, 123 (1992).
161 R. Lipton, and B. Vernescu, Critical radius, size effects and inverse problems for composites with imperfect interface, J. Appl. Phys. **79**, 8964 (1996).
162 R. Lipton, and B. Vernescu, Composites with imperfect interface, Proc. R. Soc. Lond. A **452**, 329 (1996).
163 S. Torquato, and M. D. Rintoul, Effect of the interface on the properties of composite media, Phys. Rev. Lett. **75**, 4067 (1995).
164 H. Cheng, and S. Torquato, Effective conductivity of periodic arrays of spheres with interfacial resistance, Proc. R. Soc. Lond. A **453**, 145 (1997).
165 C. W. Nan, X. P. Li, and R. Birringer, Inverse problem for composites with imperfect interface: Determination of interfacial thermal resistance, thermal conductivity of constituents, and microstructural parameters, J. Am. Ceramic Soc. **83**, 848 (1997).
166 R. Lipton, and D. R. S. Talbot, Bounds for the effective conductivity of a composite with an imperfect interface, Proc. R. Soc. Lond. A **457**, 1501 (2001).
167 D. Duschlbauer, H. E. Pettermann, and H. J. Böhm, Heat conduction of a spheroidal inhomogeneity with imperfectly bonded interface, J. Appl. Phys. **94**, 1539 (2003).
168 H. Cheng, and S. Torquato, Effective conductivity of dispersions of spheres with a superconducting interface, Proc. R. Soc. Lond. A **453**, 1331 (1997).
169 R. Lipton, Variational methods, bounds, and size effects for composites with highly conducting interface, J. Mech. Phys. Solids **45**, 361 (1997).
170 R. Lipton, Influence of interfacial surface conduction on the DC electrical conductivity of particle reinforced composites, Proc. R. Soc. Lond. A **454**, 1371 (1998).
171 E. J. Garboczi, and D. P. Bentz, Computer simulation of the diffusivity of cement-based materials, J. Mater. Sci. **27**, 2083 (1992).
172 Y. Benveniste, and T. Miloh, Neutral inhomogeneities in conduction phenomena, J. Mech. Phys. Solids **47**, 1873 (1999).
173 Z. Hashin, and S. Shtrikman, A variational approach to the theory of the effective magnetic permeability of multiphase materials, J. Appl. Phys. **33**, 3125 (1962).
174 Y. Benveniste, and T. Miloh, The effective conductivity of composites with imperfect thermal contact at constituent interfaces, Int. J. Eng. Sci. **24**, 1537 (1986).
175 Z. Hashin, Assessment of the self consistent scheme approximation: Conductivity of particulate composites, J. Composite Mater. **2**, 284 (1968).
176 S. Kamat, X. Su, R. Ballarini, and A. H. Heuer, Structural basis for the fracture toughness of the shell of the conch Strombus gigas, Nature **405**, 1036 (2000).
177 H. Gao, B. Ji, I. L. Jager, E. Arzt, and P. Fratzl, Materials become insensitive to flaws at nanoscale: Lessons from nature, Proc. Natl. Acad. Sci. USA **100**, 5597 (2003).
178 A. N. Goldstein, C. M. Echer, and A. P. Alivisatos, Melting in semiconductor nanocrystals, Science **256**, 1425 (1992).
179 G. Bertsch, Melting in clusters, Science **277**, 1619 (1997).
180 H. Miyata, T. Suzuki, A. Fukuoka, T. Sawada, M. Watanabe, T. Noma, K. Takada, T. Mukaide, and K. Kuroda, Silica films with a single-crystalline mesoporous structure, Nat. Mater. **3**, 651 (2004).
181 K. Kendall, The impossibility of comminuting small particles by compression, Nature **272**, 710 (1978).
182 B. L. Karihaloo, The impossibility of comminuting small particles by compression, Nature **279**, 169 (1979).
183 D. J. Bottomley, and T. Ogino, Alternative to the Shuttleworth formulation of solid surface stress, Phys. Rev. B **63**, 165412 (2001).
184 J. Wang, H. L. Duan, Z. P. Huang, and B. L. Karihaloo, A scaling law for properties of nano-structured materials, Proc. R. Soc. A. **462**, 1355 (2006).
185 P. Buffat, and J. P. Borel, Size effect on the melting temperature of gold particles, Phys. Rev. A **13**, 2287 (1976).
186 P. R. Couchman, and W. A. Jesser, Thermodynamic theory of size dependence of melting temperature in metals, Nature **269**, 481 (1977).
187 T. Castro, R. Reifenberger, E. Choi, and R. P. Andres, Size-dependent melting temperature of individual nanometer-sized metallic clusters, Phys. Rev. B **42**, 8548 (1990).
188 K. F. Peters, J. B. Cohen, and Y. W. Chung, Melting of Pb nanocrystals, Phys. Rev. B **57**, 13430 (1998).
189 M. Zhao, X. H. Zhou, and Q. Jiang, Comparison of different models for melting point change of metallic nanocrystals, J. Mater. Res. **16**,

3304 (2001).
190 K. K. Nanda, S. N. Sahu, and S. N. Behera, Liquid-drop model for the size-dependent melting of low-dimensional systems, Phys. Rev. A **66**, 013208 (2002).
191 K. Dick, T. Dhanasekaran, Z. Zhang, and D. Meisel, Size-dependent melting of silica-encapsulated gold nanoparticles, J. Am. Chem. Soc. **124**, 2312 (2002).
192 C. Q. Sun, Y. Wang, B. K. Tay, S. Li, H. Huang, and Y. B. Zhang, Correlation between the melting point of a nanosolid and the cohesive energy of a surface atom, J. Phys. Chem. B **106**, 10701 (2002).
193 K. K. Nanda, F. E. Kruis, and H. Fissan, Evaporation of free PbS nanoparticles: Evidence of the Kelvin effect, Phys. Rev. Lett. **89**, 256103 (2002).
194 W. A. Jesser, R. Z. Shneck, and W. W. Gile, Solid-liquid equilibria in nanoparticles of Pb-Bi alloys, Phys. Rev. B **69**, 144121 (2004).
195 P. Bergese, I. Colombo, D. Gervasoni, and L. E. Depero, Melting of nanostructured drugs embedded into a polymeric matrix, J. Phys. Chem. B **108**, 15488 (2004).

具有界面效应的复合材料细观力学

段慧玲, 王建祥, 黄筑平

摘要 复合材料中存在界面, 这些界面极大地影响了复合材料的力学和传导性能. 复合材料中界面的弹性与传导特性通常通过三种界面模型进行表征. 对于弹性问题, 这三种界面模型分别是界面应力模型(interface stress model, ISM)、线性弹簧模型(linear spring model, LSM)和界面相模型. 对于传导问题, 这三种界面模型分别是高传导(high conducting, HC)界面模型、低传导(low conducting, LC)界面模型和界面相模型. 具有界面效应的弹性问题又可以分为两类. 第一类弹性问题涉及边值问题的求解, 旨在预测具有界面效应的复合材料等效性能; 第二种弹性问题涉及表面/界面应力对纳米结构材料弹性性能的影响, 通常以界面应力模型进行表征. 本文首先回顾了具有界面效应的弹性问题的三个方面, 即三种界面模型之间的等价关系, Eshelby体系和细观力学框架. 本文着重以界面应力模型为例, 展示了如何通过将界面弹性补充到经典弹性问题的基本方程中, 将经典理论框架扩展到纳米尺度. 然后, 还回顾了具有界面效应的复合材料的传导问题, 并给出了预测复合材料等效传导性能的一般框架. 论文的最后还讨论了用于描述复合材料与尺寸相关的弹性和传导性能的标度律.